AD-A082 526 TEXAS UNIV AT AUSTIN F/G 11/6
THE INFLUENCE OF HOLD TIMES ON FATIGUE CRACK GROWTH OF ALUMINUM--ETC(U)
FEB 80 H L MARCUS AFOSR-76-2955
UNCLASSIFIED AFOSR-TR-80-0233 NL

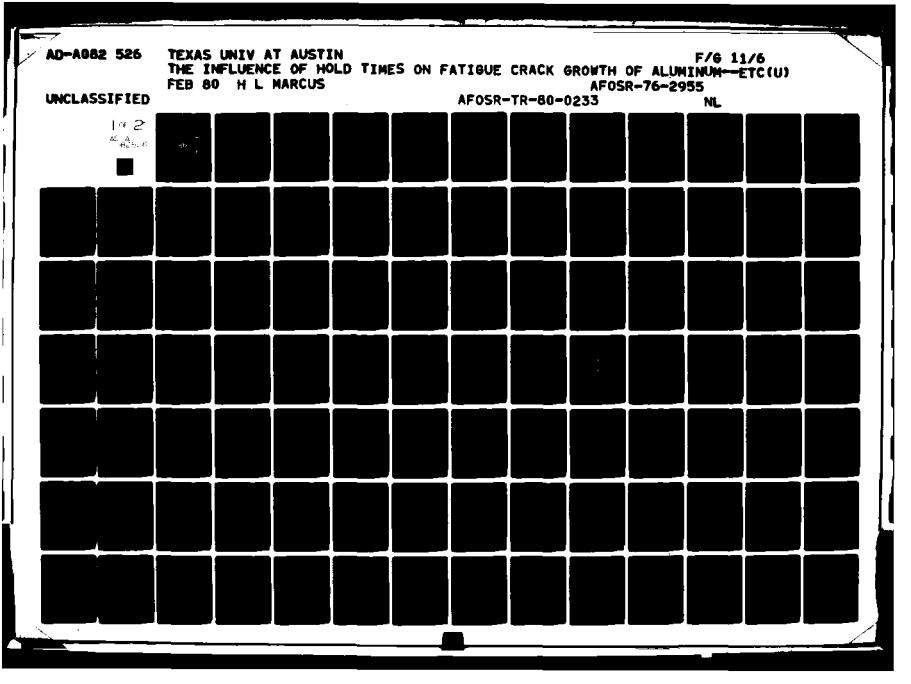

UNCLASSIFIED

SECURITY CLASSIFICATION OF THIS PAGE (When Data Entered)

REPORT DOCUMENTATION PAGE

READ INSTRUCTIONS BEFORE COMPLETING FORM

1. REPORT NUMBER: AFOSR-TR-80-0233	2. GOVT ACCESSION NO. / 3. RECIPIENT'S CATALOG NUMBER
4. TITLE (and Subtitle): THE INFLUENCE OF HOLD TIMES ON FATIGUE CRACK GROWTH OF ALUMINUM ALLOYS	5. TYPE OF REPORT & PERIOD COVERED: Final Report 1 Jan 1976 — 31 Dec 1979 / 6. PERFORMING ORG. REPORT NUMBER
7. AUTHOR(s): H.L. Marcus	8. CONTRACT OR GRANT NUMBER(s): AFOSR-76-2955
9. PERFORMING ORGANIZATION NAME AND ADDRESS: The University of Texas, Dept. of Mechanical Eng. and M.S.&E., Austin, TX 78712	10. PROGRAM ELEMENT, PROJECT, TASK AREA & WORK UNIT NUMBERS: 2306/A1, 61102F
11. CONTROLLING OFFICE NAME AND ADDRESS: Department of the Air Force, AFOSR/NE, Air Force Office of Scientific Research, Bolling AFB, D.C. 20332	12. REPORT DATE: 21 Feb 1980 / 13. NUMBER OF PAGES: 103
14. MONITORING AGENCY NAME & ADDRESS (if different from Controlling Office): 106	15. SECURITY CLASS. (of this report): Unclassified / 15a. DECLASSIFICATION/DOWNGRADING SCHEDULE: N/A

LEVEL

16. DISTRIBUTION STATEMENT (of this Report)

Approved for public release; distribution unlimited.

DTIC ELECTE APR 1 1980 S C

17. DISTRIBUTION STATEMENT (of the abstract entered in Block 20, if different from Report)

18. SUPPLEMENTARY NOTES

19. KEY WORDS (Continue on reverse side if necessary and identify by block number)

fracture, fatigue crack growth, crack closure, environmental effects, dislocation sweep-in, aluminum alloys, fatigue, ultrasonic testing, AES, SIMS, relaxation, ion implantation, hydrogen embrittlement, trapping.

20. ABSTRACT (Continue on reverse side if necessary and identify by block number)

The results of the research on fatigue crack growth in aluminum alloys are described in three general areas. The first relates the influence of hold time at an underload that follows an overload on the fatigue crack growth retardation behavior of the 7075 and 2219 aluminum alloys. A very distinct effect on retardation with hold time is observed. The effect is microstructure dependent with the time dependence

OVER

DD FORM 1 JAN 73 1473 EDITION OF 1 NOV 65 IS OBSOLETE

UNCLASSIFIED

SECURITY CLASSIFICATION OF THIS PAGE (When Data Entered)

347800

AFA082523

Block 20 con't.

behavior extending over a longer period for the high strength materials. This well-defined time dependence clearly shows that lifetime predictions based on accelerated short hold time tests could be very non-conservative. The influence of humidity was also determined using vacuum as a reference environment.

The second aspect of the research investigated the nature of the residual displacement, d, that leads to the crack closure phenomena. In this aspect of the study, d was determined using a compliance gage on the side of the specimen and the crack tip was monitored simultaneously with an acoustic transducer. Results for varying ΔK in a humid environment showed the possiblility of measuring d, using it in a finite element model to predict the crack closure load. This could then be used to predict ΔK_{eff} and ultimately fatigue crack growth. This trend was not followed when the d value was determined in a variety of environments. In fact an inverse correlation between d and crack closure and fatigue crack growth rate was observed. This was interpreted in terms of the unconstrained plane stress surface region. Measurements are also reported showing that there is closure in the interior plane strain region that is modified if the outer region is machined away. The results in the d aspect of the study was to reduce the likelihood of the use of surface measured d as a useful set of data to use in analytic lifetime predictions.

The last major emphasis was to investigate how gaseous environments interact with fatigue crack growth in aluminum alloys. Combined AES/SIMS studies were made of fracture surfaces taken from fatigue crack growth specimens fatigued in vacuum and subsequently exposed to and fatigued in a range of environments. The environments included O_2, O_2^{18}, H_2, D_2, D_2O, H_2O and N_2. The results showed a deeper penetration of oxygen during fatigue. The deuterium was trapped near the surface for the sample fatigued in D_2O but not for the sample fatigued in vacuum and subsequently exposed to D_2O. To help interpret the results, deuterium was ion implanted into an aluminum specimen with varied surface conditions including the fatigue fracture surface. The diffusion of the deuterium from the implanted distribution was monitored by combined inert ion sputtering and SIMS. The deuterium profiles obtained in the fatigue studies were reproduced by the ion implantation experiments leading to the conclusion that many strong trapping sites were produced near the fracture surface during the fatigue crack growth. A model using an image force technique was developed to explain some of the observed diffusion results for the ion implanted deuterium experiments.

INDEX

THE INFLUENCE OF HOLD TIMES ON FATIGUE CRACK GROWTH OF ALUMINUM ALLOYS

FINAL REPORT

H.L. Marcus
Departments of Mechanical Engineering and
Materials Science and Engineering
The University of Texas
Austin, Texas 78712

I. Introduction

This report will describe the results of a series of experiments whose primary aim was to clarify the fatigue crack growth behavior of aluminum alloys. The results are presented in a condensed form in the main body of the report with the details of the results in a series of appendices, which in general are either preprints or reprints of papers submitted for publication. The major literature references are also included in the write-ups in the appendices.

There were several aspects of fatigue crack growth in aluminum alloys that were investigated. The first was the study of the influence of hold time at an underload after an overload on the crack retardation behavior of the aluminum alloys. As part of this effort, the crack closure behavior of the material was observed using ultrasonic and compliance techniques. To clarify the ultrasonic technique, a study on the acoustic energy transmissions through an interface was made. A second part of the study was an attempt to identify

the cause of crack closure in terms of the nature of the material in actual contact. An added incentive to getting a direct measure of the origin of crack closure by a measurement of the amount of residual displacement was its potential use as a characteristic number for closure load prediction. This could be used for crack growth prediction using finite element methods to define ΔK_{eff}.

In order to evaluate this behavior, a series of experiments were performed in hard vacuum and a range of gaseous environments. The aluminum alloys 2219-T851 and 7075-T651 were used in the studies in the above conditions and in the lower strength level overaged condition.

To further characterize the fracture surfaces a series of secondary ion mass spectroscopy (SIMS) and scanning auger microscopy (SAM) experiments were performed on samples fatigued in gaseous environments including O^{18}, D_2O, D_2 and vacuum. Additional ion implantation SIMS studies were done to assist in evaluating the observed fatigue results.

II. The Influence of Underload Time on Overload Crack Retardation

It is well known that an overload during a constant load amplitude fatigue crack growth study will greatly retard the subsequent crack growth. In addition, an underload following the crack growth reduces the magnitude of the retardation phenomenon. In this study the influence of

hold time at an underload after an overload was investigated in 7075-T651 and 2219-T851 and in their overaged condition for a range of loading and environmental conditions. The details of these results are presented in Appendices A and B.

The main results of the underload study were the following:

1) A significant reduction in retardation due to an overload is observed for a zero load underload when the underload is held for 24 to 48 hours. If this hold time effect is not taken into account, the predicted lifetime based on the accelerated short underload time tests can be more than twice the actual life.

2) The time required for the underload to complete its relaxation is a function of the strength level of the material. For both the 2219-T851 and the 7075-T651 alloys the relaxation effect due to the underload is approximately complete after 24 hours but is significantly less when the material is overaged to significantly reduce the yield strength.

3) There is a difference in the underload hold time effect depending on whether the experiment was run in vacuum or in humid air (relative humidity between 5 and 50%) with a greater relaxation effect seen in humid air.

4) The retardation seems to be related to crack closure resulting from the crack tip being enclosed by the residual deformation and displacement from the overload. Hold time at underloads apparently reduces the magnitude of the residual displacements through some room temperature relaxation effect.

III. Ultrasonic Transmission Through A Rough Interface

In the studies reported here the measurement of crack closure using ultrasonic transducers is heavily emphasized. One of the major questions about this technique to identify the closure load is how much force across the fracture surface is required to transmit the acoustic wave. In principle, the transmission across a very thin air gap can be significant. To determine the stresses required, a series of surfaces of the aluminum alloys were prepared with a wide range in surface roughness. The ultrasonic signal transmitted through this interface was then measured as a function of applied load. The results clearly demonstrated a normal stress of the order of five to twenty percent of the yield strength was required for significant transmission of the ultrasonic wave. Virtually no signal was transmitted when the blocks lay at rest on each other. Based on these results, the details of which are given in appendix C, the ultrasonic closure measurements were considered to be realistic since a significant compressive stress was required for transmission of the signal. No attempt was made to evaluate diffraction effects on the transmitted ultrasonic wave associated with the change in crack tip shape during the loading cycle.

As an outgrowth of these measurements a model was developed to identify the true crack length using ultrasonic measurements when the crack is partially closed. To accomplish this

nondestructive evaluation of the crack length, the stress and roughness dependence of the transmitted acoustic energy is integrated to give the measured ultrasonic intensity. This approach could be used in either the transmitted or back-scattered mode. The details of the model are given in appendix D where several specific crack and transducer geometries are discussed.

IV. Evaluation of the Residual Displacement, d, Associated With Crack Closure

In the Elber model of crack closure the two fracture surfaces can come in contact during the low end of the tension cycle only if displacement above the theoretical plane of the crack exists. This residual displacement, d, has several potential origins including surface roughness, volume increase due to deformation including the constant volume effect and formation of an oxide on the surface. The constant volume effect associated with the plastic deformation will be most significant in the vicinity where the crack tip intercepts the surface of the sample. In this region the plane strain condition is relaxed and the behavior is more closely simulated by a plane stress description.

In considering how to analyze the residual displacement, several approaches were taken. In the first approach, it was assumed that if you could measure the d value, it would be

representative of the crack closure behavior. If this was true, the crack closure load could be calculated using a finite element model where the measured residual displacement was introduced onto the idealized fracture surface. A description of the measurement of d using surface clip-on gauges and the finite element model is given in appendix E. In this case the value of d was determined in a humid environment and the d value determined was found to increase with the closure load. Good agreement was found over a limited ΔK range between the ultrasonically measured crack closure load and the crack closure load calculated from the finite element model.

If this correlation between d and the crack closure load could be confirmed over a wide range of loading and environmental conditions, the possibility would then exist to measure d for any expected load history, and using the finite element analysis predict the closure load and directly be able to calculate life. In order to more closely examine this correlation a series of measurements were performed in vacuum and in humid air. The details of these experiments are given in appendix F. There were several conclusions of interest coming from these results. The first was the fact that the measured value of d determined by running the crack in the compact tension specimen through a clip-on gage mounted on the surface was inversely proportional to the crack closure load measured ultrasonically and the crack growth rate as a function of relative humidity.

This was totally opposite to what was expected. To evaluate this, a series of experiments were run measuring d and crack closure where the crack was grown in vacuum and then various gaseous environments were introduced. It was found that the d value increased dramatically when water vapor was introduced but the ultrasonically measured crack closure load was lowered. The introduction of N_2 had no effect and O_2 a very small effect. The results led to the conclusion that the humidity influenced the near surface plane stress region to a much greater extent than the interior. A possible explanation is the oxide strengthening of the asperities led to the increase in d.

This sequence of results clearly demonstrated that the concept of using surface measured d values to predict overall crack closure was not a viable approach. In fact it pointed out the extreme caution that must be used in interpreting any surface strain measurement.

Another factor in the measurement of crack closure is the question of whether it is only a plane stress phenomena. To clarify this point, crack closure was measured on a sample using ultrasonic methods. The outsides of the sample were then machined away and the closure load remeasured. The details of these measurements are given in appendix G. Crack closure was present in the ultrasonic measurements in the central plane strain region of the specimen before machining. The crack closure load was decreased when the outer plane

stress region with the high d was removed. This was due to the lack of the high d outer region propping open the center of the crack during the unloading cycle. The results clearly demonstrate that crack closure occurs in the plane strain region.

V. The Interaction of Gases with the Crack in Aluminum During Fatigue Crack Growth

The final area of investigation probing the fatigue crack growth in aluminum alloys was the attempt to evaluate the interaction between the gaseous environments and the fatigue crack. In this study an attempt was made to identify where the elements went relative to the surface. The fatigue experiments consisted of running a fatigue crack in vacuum for a short way and then introducing the gaseous environment and continuing the fatigue crack growth. The environments studied included vacuum, O_2, N_2, H_2O, D_2O, O_2, O_2^{18}, and D_2. The samples were removed from the mechanical test chamber after fatigue crack growth was completed and transferred to the SAM/SIMS system. The details for these studies are given in appendices H, I and J. In all cases inert ion sputtering combined with AES and SIMS was performed in the fracture surface formed in vacuum and subsequently exposed to the gas and on the surface formed in the gas. In the case of oxygen, it was consistently found that the oxygen penetrated deeper into the fatigue crack fracture surface than the normal oxide

thickness associated with diffusion (appendix H). This was true for the oxide formed in both gaseous oxygen or in the presence of water vapor. This extra penetration from dry oxygen did not seem to enhance the fatigue crack growth rate in the aluminum alloys, although it did in the Ti and Ni/Cu alloys that were also tested. This lack of enhanced fatigue crack growth in the aluminum alloys exposed to dry oxygen even though the oxygen was deeper into the surface could be an indication that in the case of water vapor the enhanced crack growth rate is probably not associated with the enhanced oxygen presence. This would leave the hydrogen originating from the water as the element most likely enhancing the fatigue crack growth of the aluminum alloys.

In order to evaluate the region of hydrogen interaction, SAM/SIMS studies were performed on the fracture surface of the alloys fatigued first in vacuum and then in D_2O. The deuterium was used as a marker to control hydrogen contamination arising during the transfer between the fatigue environmental chamber and the SAM/SIMS vacuum chamber. The SAM was used to monitor the oxygen peak and the SIMS the deuterium peak during the inert ion sputtering (appendix I). The results for the D_2O measurements show a much greater penetration of deuterium into the fracture surface created during exposure to D_2O than the segment exposed to D_2O after the fatigue crack was formed.

The results were obtained about 24 hours after the fatigue crack growth took place. If there were no strong trapping sites available for the deuterium, it should have diffused out of the aluminum alloys during the time of fatiguing and transfer. In order to investigate the presence of trapping sites, a series of deuterium ion implantation experiments were performed on the 7075 and 2219 alloys that were initially in the unrolled, rolled, fatigue fracture surface and unrolled but damaged by high energy neon ion implantation prior to the time of the deuterium ion implantation. For the details of the results and analysis, see appendix J. The deuterium profiles obtained could be broken into two categories. The first was for the unrolled specimen, with and without neon ion induced damage. In these cases the results were controlled by the surface oxide acting as a diffusion barrier. To interpret this behavior, an image force model for diffusion across the oxide surface was developed. The results of the model closely correlated with the experimental results. The second type of result was obtained for the fatigued fracture surfaces and the cold worked surfaces. In this case, the deuterium profiles were very similar in depth beyond the oxide to that found in the samples fatigued in D_2O. The profiles in the fatigued fracture surfaces associated with the implanted deuterium were formed by diffusion toward the surface with the trapping sites

filling during the exit of the deuterium. The samples fatigued in D_2O resulted in deuterium profiles where the deuterium originates at the crack tip. The fact that both resulted in similar profiles can be interpreted to mean that the observed distribution is representative of the strong trapping sites distribution. This distribution during fatigue can influence the fatigue crack growth rate, but the mechanism of its influence is not modeled at present.

VI. Summary

The results of the research on fatigue crack growth in aluminum alloys are described in three general areas. The first relates the influence of hold time at an underload that follows an overload on the fatigue crack growth retardation behavior of the 7075 and 2219 aluminum alloys. A very distinct effect on retardation with hold time is observed. The effect is microstructure dependent with the time dependence behavior extending over a longer period for the high strength materials. This well-defined time dependence clearly shows that lifetime predictions based on accelerated short hold time tests could be very non-conservative. The influence of humidity was also determined using vacuum as a reference environment.

The second aspect of the research investigated the nature of the residual displacement, d, that leads to the crack closure phenomena. In this aspect of the study, d was determined

using a compliance gage on the side of the specimen and the crack tip was monitored simultaneously with an acoustic transducer. Results for varying ΔK in a humid environment showed the possibility of measuring d, using it in a finite element model to predict the crack closure load. This could then be used to predict ΔK_{eff} and ultimately fatigue crack growth. This trend was not followed when the d value was determined in a variety of environments. In fact an inverse correlation between d and crack closure and fatigue crack growth rate observed. This was interpreted in terms of the unconstrained plane stress surface region. Measurements are also reported showing that there is closure in the interior plane strain region that is modified if the outer region is machined away. The results in the d aspect of the study was to reduce the likelihood of the use of surface measured d as a useful set of data to use in analytic lifetime predictions.

The last major emphasis was to investigate how gaseous environments interact with fatigue crack growth in aluminum alloys. Combined AES/SIMS studies were made of fracture surfaces taken from fatigue crack growth specimens fatigued in vacuum and subsequently exposed to and fatigued in a range of environments. The environments included O_2, O_2^{18}, H_2, D_2, D_2O, H_2O and N_2. The results showed a deeper penetration of oxygen during fatigue. The deuterium was trapped near the surface for the sample fatigued in D_2O but not for the sample fatigued

in vacuum and subsequently exposed to D_2O. To help interpret the results, deuterium was ion implanted into an aluminum specimen with varied surface conditions including the fatigue fracture surface. The diffusion of the deuterium from the implanted distribution was monitored by combined inert ion sputtering and SIMS. The deuterium profiles obtained in the fatigue studies were reproduced by the ion implantation experiments leading to the conclusion that many strong trapping sites were produced near the fracture surface during the fatigue crack growth. A model using an image force technique was developed to explain some of the observed diffusion results for the ion implanted deuterium experiments.

Appendix A

THE INFLUENCE OF UNDERLOAD TIME ON CRACK GROWTH RETARDATION OF ALUMINUM ALLOYS

Granville Sewell and H. L. Marcus
Mechanical Engineering/Materials Science and Engineering
The University of Texas at Austin
Austin, Texas 78712 USA
tel: 512/471-1136

It is now well known that an overload applied during a metal fatigue crack growth experiment causes crack growth retardation [1,2,3]. In addition, underloads subsequent to the overload tend to reduce the retardation phenomena [1]. It has been reported that time at small underload does not seem to play a significant role in its influence on the retardation behavior [3]. The data presented here, however, where the underload is greater, do show such a time effect. This question is of particular significance in terms of relating accelerated laboratory tests to the actual loading seen during the service lifetime of a structure designed to the fatigue crack growth behavior of the material.

Fatigue crack growth experiments were carried out on an Al 2219-T851 (σ_Y = 50 ksi) compact tension specimen (B = 1 in, W = 4.25 in, H = 2.09 in). Baseline tension-tension loading consisted of a 10 Hz sine wave whose mean value and amplitude are varied so that at each point where an overload is applied (4 points per sample, spaced 3/8 in apart), K_{min} = 4 ksi$\sqrt{in}$ and K_{max} = 12 ksi$\sqrt{in}$. The overload is such that $K_{overload}$ = 30 ksi$\sqrt{in}$ ($K_{Ic} \cong$ 40 ksi$\sqrt{in}$). Testing is done on an MTS closed loop electro-hydraulic testing machine, in room air with relative humidity between 30% and 55%.

Crack depth is plotted versus number of cycles. The extension of the steady-state growth lines before and after the overload should be roughly parallel, with a separation of a certain number of cycles which we will call the delay.

The relative crack depth is measured by the attenuation of a transmitted longitudinal ultrasonic wave, transmitted and received by two 2.25 MHz piezoelectric transducers. The received signal is converted to a DC signal and is plotted against load. This plot is not only a means of monitoring crack growth, but also shows the crack closure effect reported in [2,3,4], that is, that the crack effectively closes at loads below some $P_c > P_{min}$.

An underload of varying magnitude and duration was applied after each overload. Each test was repeated three times, never twice on the same sample or at the same crack length. Results are summarized in Figs. 1 and 2.

The extent of the retardation delay decreases with the time at zero load (Fig. 1) and also with the magnitude of the underload (Fig. 2). The significant result shown here is the influence of holding time at zero load. A decrease of about 50% in retardation delay is caused by an underload of about 2 sec. Extending the hold time to 24 hr reduces this by about another 30%. The impact on design philosophy would be even greater if the 2 sec hold time represents the accelerated tests and the 24 hr represents the real loading history.

Int Journ of Fracture 13 (1977)

Using the crack closure model [2,4], what happens is that when baseline loading is resumed, the crack is not fully open and the crack growth rate is reduced and will not return to the steady-state value until the two rough crack surfaces created during the overload become smooth through cyclic contact. During the underload, these two surfaces are smoothed as they are pressed together. Time at underload then increases this smoothing due to a strain relaxation process.

Additional experimental effort is now being performed to determine the influence of strength level, microstructure, humidity, and other loading histories on this relaxation behavior, and an attempt will be made to model the strain relaxation phenomena.

Acknowledgments: This research is sponsored by the Air Force Office of Scientific Research, Air Force Systems Command, USAF, under Grant No. AFOSR 76-2955.

REFERENCES

[1] R. I. Stephens, D. K. Chen, B. W. Hom, *Fatigue Crack Growth Under Spectrum Loads*, STP 595, American Society for Testing and Materials, Philadelphia (1976) 27-40.

[2] Otto Buck, J. D. Frandsen, J. L. Marcus, *Fatigue Crack Growth Under Spectrum Loads*, STP 595, American Society for Testing and Materials, Philadelphia (1976) 101-112.

[3] W. N. Sharpe, Jr., D. M. Corbly, A. F. Grandt, Jr., *Fatigue Crack Growth Under Spectrum Loads*, STP 595, American Society for Testing and Materials, Philadelphia (1976) 61-77.

[4] W. Elber, *Damage Tolerance in Aircraft Structures*, STP 486, American Society for Testing and Materials, Philadelphia (1971) 230-242.

19 January 1977

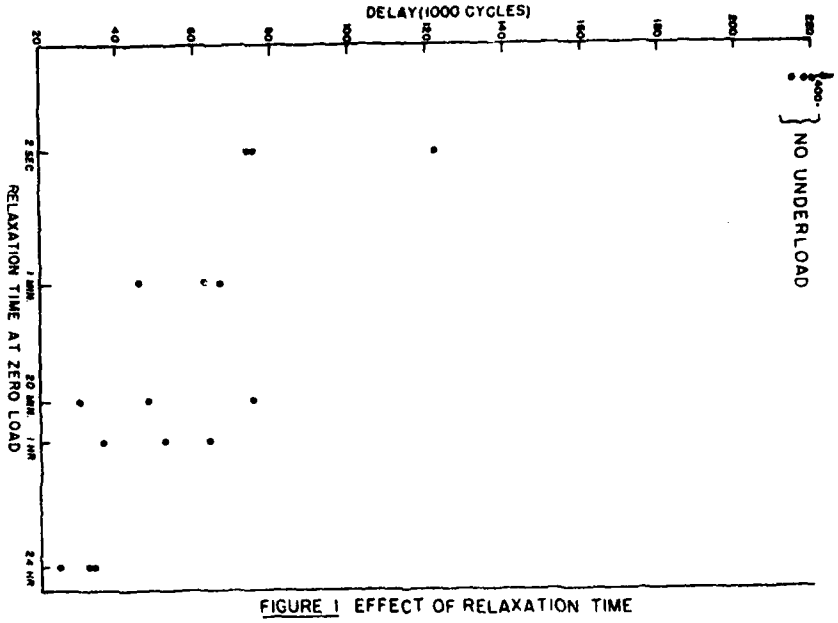

FIGURE 1 EFFECT OF RELAXATION TIME

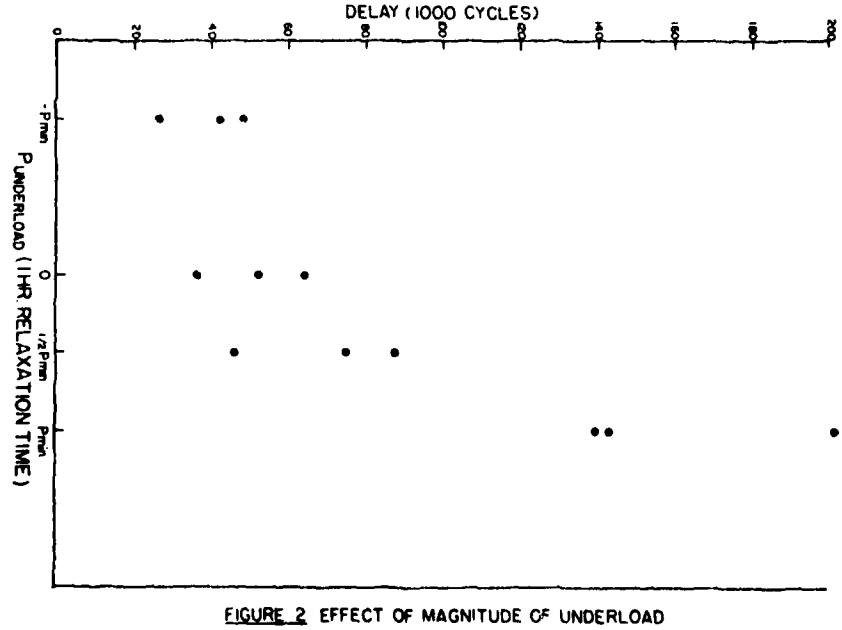

FIGURE 2 EFFECT OF MAGNITUDE OF UNDERLOAD

Appendix B

Effect of Hold Times on Crack Retardation In Aluminum Alloys

W.P. Slagle, Deepak Mahulikar
and H.L. Marcus
Department of Mechanical Engineering and
Materials Science and Engineering
The University of Texas
Austin, Texas 78712

Introduction

The phenomenon of crack retardation following an overload has been studied extensively[1-4]. It is also reported in the literature that an underload following an overload tends to reduce the retardation phenomenon[4-6]. Effects of hold times on this reduction in delay have also been investigated to a certain extent[6-7]. Such time effects could be significant in correlating laboratory data from accelerated life tests to real life fatigue performance of engineering structures.

In this investigation, hold time effects on fatigue crack retardation in two high strength aluminum alloys, 2219 and 7075, were studied. Influences of different metallurgical conditions and different environments were examined.

Many of the observations in this research will be discussed in terms of crack closure model proposed by Elber[8] and in terms of strain relaxation effects proposed elsewhere [9,10]. It has been suggested that underloads following overloads reduce retardation due to strain relaxation at the crack

tip[9]. This phenomenon can take place due to dislocation cross slip[10]. In that case longer hold times should cause shorter delay periods which was observed by Sewell[6,9]. But Sharpe et al[7] found only a slight correlation between hold time at zero load and the number of delay cycles [N_D] while Chanani[11] reported no trend between N_D and hold time at mean load following an overload.

An aggressive environment can affect the extent of plastic deformation. Retardation is expected to increase in vacuum or dry atmospheres as compared to moist air. This trend was reported by Sewell[14]. Buck et al[12] observed lower values of ΔK_{eff} in dry nitrogen than in moist air.

Sewell and Marcus[6] report experiments where each overload was followed by one hour relaxation at an underload of variable magnitude. The results indicated that there was a reduction in delay with increasing magnitude of underload. In low humidity (<5%RH) experiments, they observed that all the phases of crack growth experiments slowed down. These include steady state crack growth and crack growth following any overload-underload combination. A decrease in delay with increase in holding time at zero load was again evident.

Because of these conflicting results it became necessary to study the effect of hold times on the retardation phenomenon. This investigation concerns with hold time experiments in vacuum and humid air for aluminum alloys with different

metallurgical treatments. Crack growth and retardation data was obtained for various hold times. The results are then interpreted in terms of crack closure model.

Experimental Procedure

Experiments were performed on the aluminum alloys 7075-T651 and 2219-T851, as well as overaged 7075 and 2219. The mechanical properties are given in Table 1. Experiments were carried out in humid air and in a hard vacuum system (0.1 μPa).

The experiments were performed on compact tension specimens with B = 2.54 cm., W = 10.8 cm and H = 5.3 cm. The specimens had a T-L orientation. An MTS closed loop electro-hydraulic fatigue testing machine was used for loading. All the cycling was sinusoidal tension-tension at a frequency of 10 Hz for a constant range in stress intensity, ΔK, and load ratio, R. Crack closure and crack growth was measured using 2.25 MHz longitudinal ultrasonic waves in transmission. The details of the technique are described elsewhere[9,12,13]. A clip on gage at the crack mouth was also used to monitor closure and growth.

The actual relaxation experiments were performed by first growing the crack for at least 48 mm before each overload. This allowed the crack to reach its steady state crack growth rate for the applied ΔK and allowed the plastic zone to stabilize. During the preliminary growth, the ultrasonic intensity

was periodically recorded along with the number of cycles N. At a predetermined crack length, an overload K_{OL}, was applied at approximately 0.1 Hz followed immediately by an underload to zero. The load was maintained at zero for a specified hold time and then raised to the mean load whereupon baseline cycling was resumed. Immediately following the overload, crack retardation was observed and the ultrasonic signal would remain constant. After several thousand cycles crack growth would start again and the retardation measurements would be made until steady state da/dN was resumed. The number of delay cycles, N_D, was then determined using a tangent method[10].

Four overloads spaced 9.5 mm apart were applied to each specimen. This distance was chosen on the basis of observations by Wei[14] which indicates no interaction effect for a distance greater than 13 times the size of the plastic zone. To minimize any possible interaction effects, the tests were varied so that no hold time was repeated on the same specimen or at the same crack length. The overloads were applied at crack lengths of 2.7 cm, 3.65 cm, 4.6 cm and 5.56 cm so that all tests were performed in the range $0.25<a/w<0.51$.

Load Parameters

1. Humid air: The 7075 alloy experiments were conducted with loading parameters of K_{min} = 3.3 MPa$\sqrt{m}$, K_{max} = 9.9 MPa$\sqrt{m}$ and

K_{OL} = 22 MPa$\sqrt{m}$. The 2219 alloy experiments were performed with K_{min} = 4.9 MPa$\sqrt{m}$, K_{max} = 13.2 MPa$\sqrt{m}$ and K_{OL} = 29.7 MPa$\sqrt{m}$. Hold times were with K = 0.

2. Vacuum: The retardation experiments were repeated in 0.1 μPa vacuum for 7075-T651 alloy. The load parameters were K_{min} = 1.1 MPa$\sqrt{m}$, K_{max} = 11 MPa$\sqrt{m}$ and K_{OL}= 22 MPa$\sqrt{m}$. This larger value of ΔK was used since crack growth was significantly slower in the vacuum environment.

Results and Discussion

Humid air: The data from 7075-T651 alloy experiments appears in Fig. 1. Without an underload, the delay times were so long (over 300 K cycles) that the tests were aborted before the crack started propagating again. These long delay times were probably due to large plastic deformation at the crack tip caused by the K_{OL} which was very close to K_{1C} of the material. Application of an underload to zero immediately following an overload caused a great reduction in the number of delay cycles, and holding the 7075 specimen at the underload reduced N_D even more. A steady reduction in retardation was observed as the hold time was increased, and it seemed to level off after 24 hours.

In the overaged 7075, most of the reduction in the retardation due to overload occurred immediately. A two-second hold time at zero load caused a significant decrease in delay. Only

a small further decrease was observed as the hold time increased. The indication was that relaxation effects occurred more quickly in the lower strength 7075 overaged material.

The data for 2219 alloys is presented in Fig. 2. The results show that for both 2219-T651 and overaged 2219 alloys, a substantial decrease in retardation due to the application of an underload after the spike is observed. This trend was similar to that in 7075 alloys. The N_D values for no underload for the overaged 2219 were less than those for the T851. Reduction in N_D for the hold time experiments showed a similar trend.

Vacuum: The overload followed by zero load hold time data for 7075-T651 alloys in 0.1μPa vacuum is presented in Fig. 3. Again, as in the humid air tests, there was a significant reduction in delay cycles with increasing time at underload.

More relaxation seemed to occur in humid air hold time tests than in vacuum tests. This may have been partially due to differences in loading conditions of vacuum and humid air, but nevertheless the results do indicate that relaxation effects are significant in vacuum but are not as great as in humid air.

Strain Relaxation

The above results can be explained in terms of strain relaxation in the vicinity of the crack tip. The dislocation cross slip mechanism which results in relaxation, is less active in vacuum than in more aggressive environments like humid air[10]. Overaging causes a significant decrease in the

delay times compared to the high strength probably due to the residual strain at the crack tip relaxing out more easily for the lower strength materials. Sanders et al[16] suggest that because of coarsening of the dispersoids, over-aging may reduce the number of secondary cracks at the main crack front resulting from fracture at particle matrix interface. This decrease in crack branching causes stress intensity at the main crack tip to increase resulting in faster crack propagation and decrease in delay.

Crack Closure

If strain relaxation is occurring in the vicinity of crack tip during overload-underload cycle, then it should cause a noticeable change in crack closure load. To verify this, experiments were carried out on overaged 2219 alloys with load parameters mentioned earlier. The ultrasonic observations are shown in Fig. 4. These closure curves indicate that at the beginning of the delay period immediately following the overload-underload sequence, the closure curve is almost completely vertical (N = 171000). Here the crack tip is completely closed, but the material which has been plastically strained by the overload is preventing the crack surfaces from closing any further. As cycling continues, the shape of the curves begin to change. The curves first begin to shift to the left indicating that the tip is just beginning to open at the higher position of the load cycle. Two inflexion points become apparent

indicating the crack closes a short distance. Soon the bottom of the curve smooths out. A well defined closure load becomes evident and it decreases with cycling to pre-overload value.

The closure data presented here seems to indicate that overload strained material which has been wedging the crack surfaces apart has been gradually hammered down. If this noticeable change in closure curves does imply hammering, it should show up on the fracture surface also. To look for such hammering, cross sections of the fracture surface of the 2219-T851 specimen were examined with an optical microscope. The overload region appears to be smoothed down or smashed down as compared to fast fracture region. This gives some visual evidence of hammering.

Thus delay after overload-underload cycle is associated with noticeable change in closure behavior of the crack tip. Although it is not clear whether the closure observations were a cause or an effect of crack behavior, the measurements were useful in studying changes at the crack tip during holding at zero load.

Conclusions

1. As hold time at zero load increased the number of delay cycles decreased for 7075-T651, 2219-T851 and overaged 7075 and 2219 alloys in humid air. This was also true for 7075-T651 alloy in vacuum. This may be due to a

time dependent strain relaxation of the residual strain created by the overload.

2. The relaxation effects were greater in humid air than in vacuum.
3. For the same load spectra, the overaged alloys exhibited shorter retardation times than high strength alloys.
4. The delay periods for 7075-T651 in vacuum were significantly higher than in humid air.
5. Changes in crack closure during retardation indicate that surface hammering may be occurring during retardation.

Acknowledgement

This research was sponsored by the Air Force Office of Scientific Research under Grant No. AFOSR 76-2955.

References

1. Wei, R.P. and Shih, T., Int. J. of Fract., 10, 1974, p.77.
2. Buck, O., J.D. Frandsen, H.L. Marcus, ASTM STP595, 1976, p. 101.
3. D.M. Corbly, P.F. Packman, Engg. Fract. Mech., 5, 1973, p. 479.
4. Jonas, O., R.P. Wei, Int. J. of Fract. Mech., 7, 1971, p. 116.
5. Stephens, R. I., D.K. Chen, B. W. Hom, ASTM STP595, 1976, p. 27.
6. Sewell, G., H.L. Marcus, Int. J. of Fract. 13, (1977), p. 247.
7. Sharpe, Jr. W.N., D.M. Corbly, A.F. Grandt Jr., ASTM STP595, 1976, p. 61.
8. Elber, W., ASTM STP 486, (1971), p. 230.
9. Sewell, G., Master's Thesis, The University of Texas at Austin, 1977.
10. Buck, O., C.L. Ho, H.L. Marcus, Engg. Fract. Mech. 5, 1973, p. 23.
11. Gallagher, J.P. and T.F. Hughes, AFFDL-TR-74-27, 1974.
12. Buck, O., J.D. Frandsen, H.L. Marcus, Engg. Fract. Mech., 7, 1975, p. 167.
13. Slagle, W. Master's Thesis, The University of Texas at Austin, 1979.
14. Wei, R.P., T.T. Shih, J.H. Fitzgerald, NASA CR-2239, 1973.
15. Hertzberg, R.W., Deformation and Fract. Mech. of Engg. Mat., John Wiley Press, 1976.
16. Sanders, J.H., Sawtell R.R., J.T. Staley, R.J. Bucci, A.B. Thoakker, NADC N0019-76-C-0482, 1976.

TABLE 1

MATERIALS	YIELD STRESS MPa	K_{1C} $MPa\sqrt{m}$
7075-T651	505	25
OVERAGED 7075	345	26
2219-T851	350	35
OVERAGED 2219	200	36

Fig.1

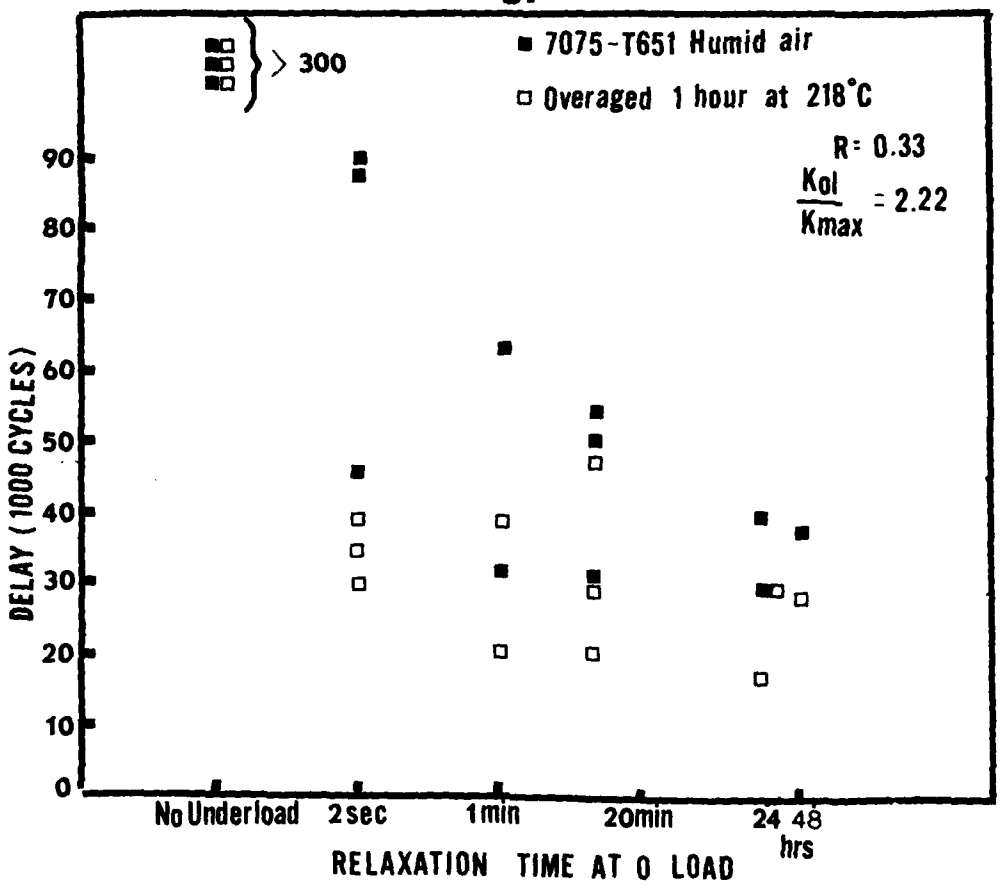
> 300
■ 7075-T651 Humid air
□ Overaged 1 hour at 218°C
R = 0.33
Kol / Kmax = 2.22
DELAY (1000 CYCLES)
90
80
70
60
50
40
30
20
10
0
No Underload
2sec
1min
20min
24 48 hrs
RELAXATION TIME AT 0 LOAD

Fig.2

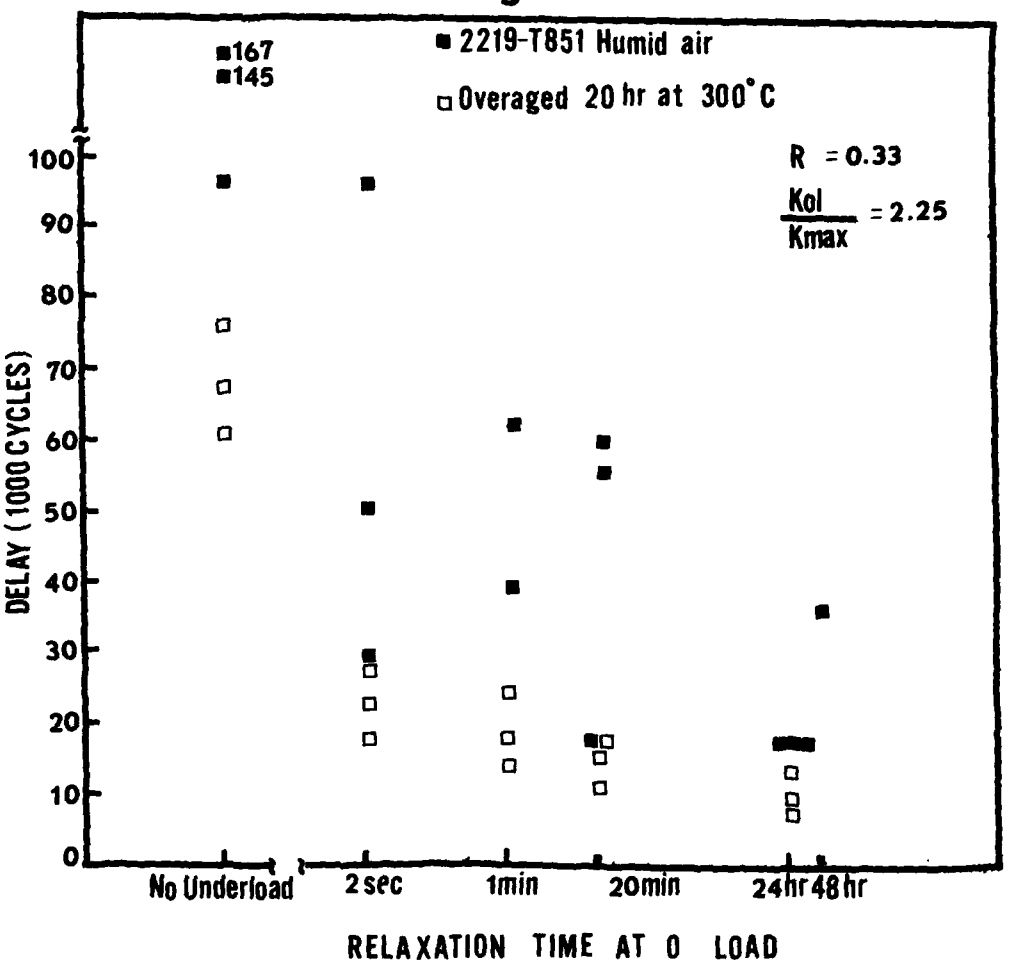
■167
■145
■ 2219-T851 Humid air
□ Overaged 20 hr at 300°C
R = 0.33
Kol / Kmax = 2.25
DELAY (1000 CYCLES)
100
90
80
70
60
50
40
30
20
10
0
No Underload
2 sec
1 min
20 min
24 hr
48 hr
RELAXATION TIME AT 0 LOAD

Fig.3

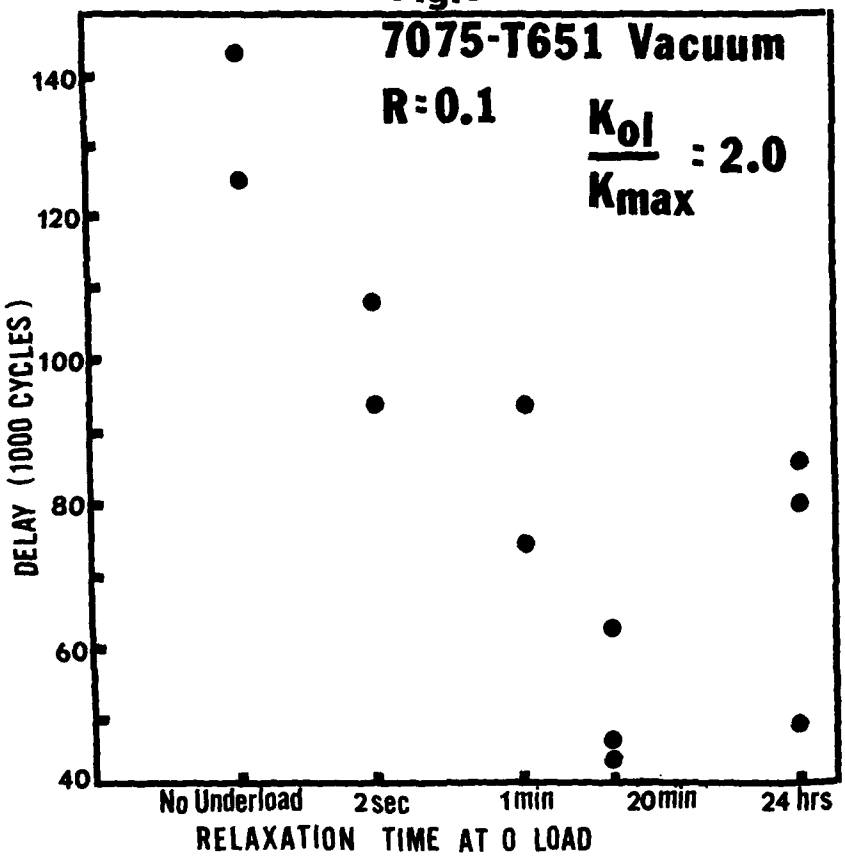
7075-T651 Vacuum
R=0.1
$\frac{K_{ol}}{K_{max}}$: 2.0
DELAY (1000 CYCLES)
140
120
100
80
60
40
No Underload
2sec
1min
20min
24 hrs
RELAXATION TIME AT 0 LOAD

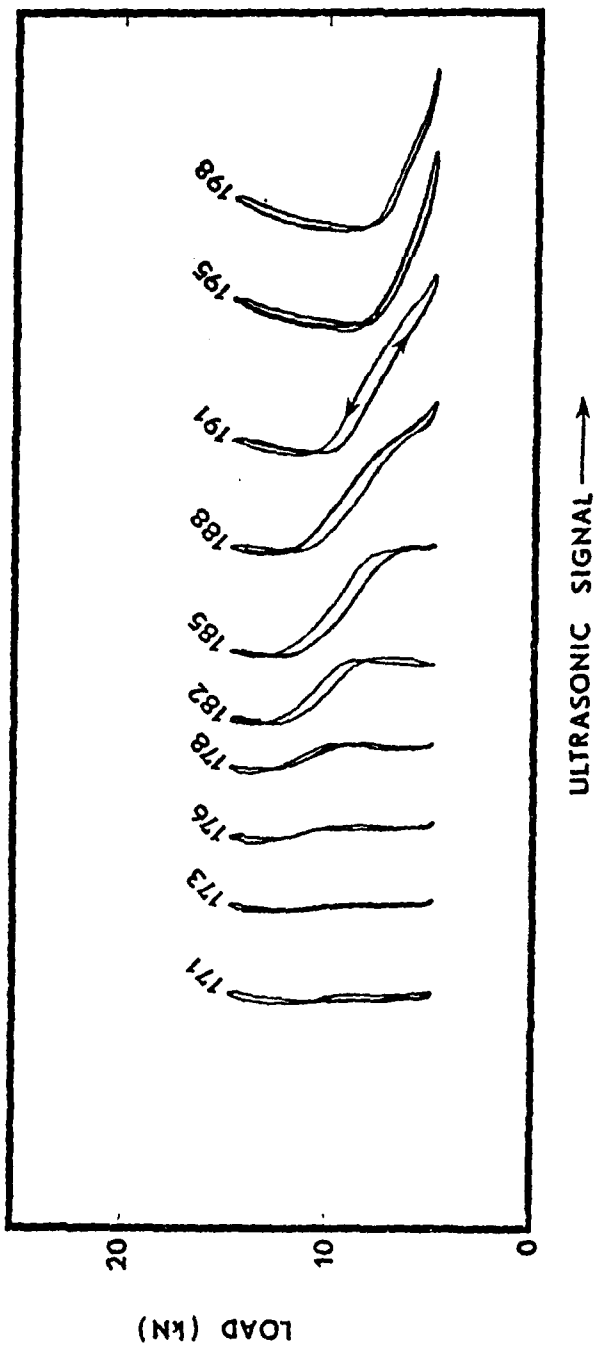
198
195
191
188
185
182
178
176
173
171
ULTRASONIC SIGNAL
20
10
0
LOAD (kN)

Fig. 4

Scripta METALLURGICA Vol. 11, pp. 521 524, 1977 Pergamon Press, Inc.
Printed in the United States

Appendix C

A MODEL FOR FATIGUE CRACK CLOSURE BASED ON SURFACE ROUGHNESS AND RESIDUAL STRAIN

GRANVILLE SEWELL and H. L. MARCUS
Mechanical Engineering/
Materials Science and Engineering
University of Texas
Austin, Tx. 78712
(Received April 18, 1977)

Introduction

The crack closure model, first developed by Elber (1), attempts to explain spectrum-loading fatigue crack growth in terms of the effective stress intensity range, ΔK_{eff}. According to this model, as a fatigue crack grows, it leaves behind a wake of residual strain (Figure 1) which may cause the crack surfaces to touch during the lower part of a tension-tension loading cycle. This crack closure has been observed experimentally (1,2,3,4). It is thought that once the surfaces touch there is no longer a singularity in the stresses at the crack tip, i.e., the stress intensity is zero. Thus the effective stress intensity range, which determines the crack growth rate, should be calculated from the effective load range, that is, the range of loads for which the crack is open, so that $\Delta K_{eff}=C(P_{max}-P_{open})$, where P_{open} is the load at which the crack opens and C is the geometrical constant relating stress intensity to load. C is a function of the crack length.

Computer Model for Crack Closure

In this section we develop a computer model for crack closure during constant amplitude loading. The computer model will be used to predict the opening load and the extent of closure at lower loads. The comparison of these predictions with experiment is given in the next section.

Assume that a fatigue crack growth experiment is carried out on a compact tension specimen with loading controlled so as to maintain constant K_{min} and K_{max}. As the crack grows, it will leave behind an approximately uniform wake of residual strain, that is, the material near the crack surfaces will effectively become thicker, because of the surface roughness and volume change associated with plastic deformation by high tensile stresses near the crack tip before final seperation. The increase in the thickness can be modeled as due to a uniform coating of thickness d of new material on the crack surfaces (Figure 1). Extending in front of the crack tip (B) for a distance equal to the plastic zone size r_y=BC, there will also be "extra material", decreasing in thickness from 2d at the tip to zero outside the plastic zone. If this "extra material" were cleared away the new crack surfaces (we will call them the "model crack" surfaces) would just touch without exerting any forces on each other when the external load, P, is removed.

Thus our model consists of a sample with a "model crack", longer than the true crack by a distance r_y, with some incompressible external material inserted between the crack surfaces propping them open. The true crack may actually be closed a distance AB behind the true crack tip, with AB depending on the external load.

For a given load, P, we use a finite-element elastic stress analysis program written by one of the authors (5) to find the stress state of the sample. One of the most important features of this program, which will be available through the algorithms distribution service

of (5), is its ability to efficiently handle crack problems. If we knew the closure distance beforehand, we could give the following boundary conditions along the model crack surfaces: From the point of closure (A) on out away from the crack tip, we know that the surfaces are free surfaces. From the point of closure on in towards the crack tip, we know the displacements, namely, from A to B the surfaces are displaced vertically by a distance d, and from B to C the displacements decrease from d to 0. In our model they decrease as a cubic polynomial with zero slope at B and C, i.e., as $d(3s^2-2s^3)$ where $s=(C-x)/(C-B)$.

Unfortunately we cannot determine the closure distance AB before solving the problem, so we proceed by an iterative method. If our guess for AB is short, this means we are allowing part of the crack surfaces to be free which would in reality be touching, so our resulting calculations will show that the true crack surfaces overlap behind the assumed point of closure. If our guess is long, this means we are glueing part of the surfaces together that would in reality not be touching, so that the true crack will be open behind the assumed point of closure. The assumed point of closure will be in compression or tension depending on whether the guess is short or long, respectively, but the stresses are not calculated as accurately as the displacements, so we do not use them to guide the iteration.

A series of computations were made with the program, for a compact tension sample with W=0.108m, H=0.053m, thickness=0.025m, $E=7.3\times10^4 MN/m^2$ and $\nu=0.33$ with plane strain conditions. The true crack length was taken as a=0.056m with a plastic zone size of $r_y=0.0014$m and a value for d of 25μm was used. The loads corresponding to three closure distances are found by iteration and tabulated below.

TABLE 1
Loads for Three Closure Distances (d=25μm)

Closure (AB)	Load (P)
0.0111m	-45 kg
0.0056m	320 kg
0 (just open)	1840 kg

The linearity of the problem implies that the values of d and P may be multiplied by a common factor without changing the closure distance. Thus for this problem, with the given crack length, our model predicts an opening load of 7.23×10^7*d kg, if d is in meters. Also, by interpolation, we see that the closure distance should be about 0.010m for zero applied load, regardless of the value of d.

The vertical stress distribution along the closure surfaces and into the plastic zone is shown for P= -45 kg in Figure 2.

Comparison of Computer Simulation with Experimental Results

To check the crack closure predictions given in the previous section, two Al-2219-T851 compact tension specimens of the same dimensions and elastic properties as in the computer simulation were tested on an MTS closed-loop electrohydraulic testing machine, after overaging for 20 hours at 300°C in air. Tensile specimens given the same heat treatment were found to have yield strengths of about 200 MN/m^2. One purpose of the lowering of the yield strength was to give a larger and more easily measureable value of d, the residual strain parameter.

In each of the two samples tested, a fatigue crack was grown to a=0.056m with loading controlled so that $K_{min}=0$ and K_{max} were held approximately constant. An extensiometer was placed so as to straddle the crack (at a=0.044m, point C of Figure 3) as it was grown through. The increase in distance between the legs of the extensiometer as the crack passed between them (distance always measured with the crack closed) is taken to be the residual strain, 2d (Figure 4), since the legs are far enough apart to straddle all the plastic strain and crack front roughness. To determine the opening load, P_{open}, and the loads P_B and P_C at which the crack closes to points B and C of Figure 3 (representing closure of 0.0056m and 0.0111m respectively), ultrasonic transducers were placed in succession at positions 1, 2 and 3. The two piezoelectric transducers transmit and receive a 2.25 megahertz longitudinal ultrasonic wave which is converted to a DC signal. This signal is attenuated as the crack grows through the path of the wave (see reference 4), so that in position 1, the signal increases when the crack first begins to close and in positions 2

or 3 the signal is zero until the crack closes to point B or C respectively. Figure 5 shows the signal as a function of load for each position of the transducer. Both Figures 4 and 5 are copied directly from the X-Y recorder output.

Loading of the first sample was a 2-hertz sine wave with K_{max}=26.4 MPa$\sqrt{m}$. The plastic zone size is estimated as $r_y=(K_{max}/\sigma_y)^2/4\sqrt{2}\pi$ =0.0010m (6). The value of d measured by the extensiometer was 8.1μm, which makes it possible to calculate the computer predictions for P_{open}, P_B and P_C by linearity.

The second sample was loaded with a 5-hertz sine wave with K_{max}=13.2 MPa$\sqrt{m}$, and d was measured as 2.5μm. The experimental results for both samples are compared with the corresponding computer predictions below, ignoring the fact that the plastic zone size for the second sample is four times smaller than for the first sample.

TABLE 2
Experimental and Calculated Closure Loads

		Experimental (±50 kg)	Calculated (d=8.1μm)
First Sample	P_{open}	450 kg	590 kg
	P_B	100 kg	100 kg
	P_C	0	-15 kg
		Experimental (±20 kg)	Calculated (d=2.5μm)
Second Sample	P_{open}	150 kg	180 kg
	P_B	50 kg	30 kg
	P_C	-100 kg	-5 kg

Discussion

The computer predictions of the opening load and extent of closure at lower loads for a crack in a compact tension specimen showed close agreement with the experimental measurement.

The elastic analysis shows that the opening load increases as d, a measure of the residual strain and crack surface roughness, increases. This is consistent with the crack closure model explanation of the well-known effects of overloads (3,4,7,8,9) and underloads (7,10). The effect of an overload is to generate a large amount of residual strain (3,4) which causes the crack to close at a higher load when baseline loading is resumed and thus ΔK_{eff} is decreased and crack growth is retarded. A subsequent underload has the opposite effect, by decreasing the residual strain through compression, and thus increasing ΔK_{eff} and the crack growth rate.

Acknowledgment

This research was sponsored by the Air Force Office of Scientific Research, Air Force Systems Command, USAF, under Grant No. AFOSR 76-2955.

References

1. W. Elber, ASTM STP 486, 230 (1971).
2. O. Buck, C.L. Ho, H.L. Marcus, Engineering Fracture Mechanics 5, 23 (1973).
3. O. Buck, J.D. Frandsen, H.L. Marcus, ASTM STP 595, 101 (1976).
4. W.N. Sharpe Jr., D.M. Corbly, A.F. Grandt Jr., ASTM STP 595, 61 (1976).
5. G. Sewell, to appear in Transactions on Mathematical Software.
6. F.A. McClintock, G.R. Irwin, ASTM STP 381, 84 (1965).
7. R.I. Stephens, D.K. Chen, B.W. Hom, ASTM STP 595, 27 (1976).
8. O.E. Wheeler, General Dynamics Report FZM 5602 (1970).
9. C.M. Hudson, H.F. Hardrath, NASA TN D-960 (1961).
10. R.I. Stephens, G.W. McBurney, L.J. Oliphant, International Journal of Fracture 10, 587 (1974).

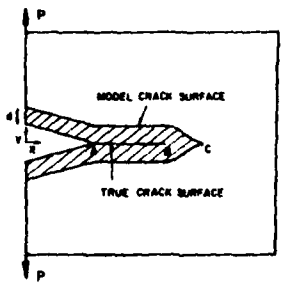

FIG.1
Model for Computer Simulation of Crack Closure

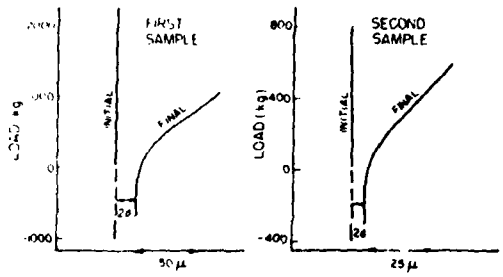

FIG.4
Experimental Measurement of d

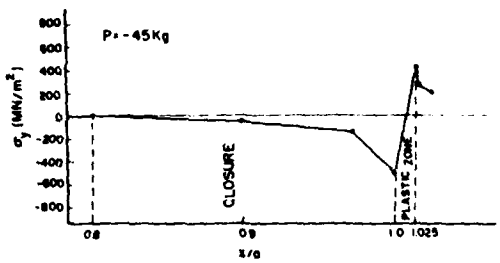

FIG.2
Stress Distribution for 0.0111m Closure

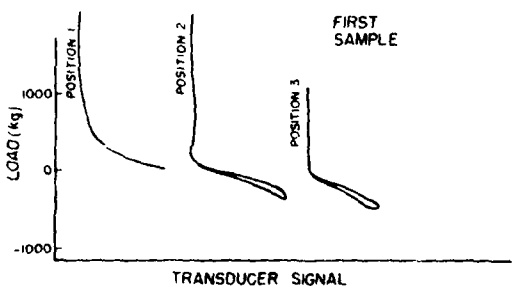

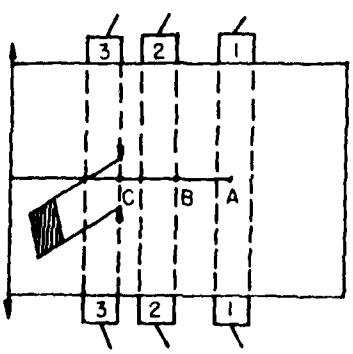

FIG.3
Extensiometer and Transducer Locations Relative to Crack

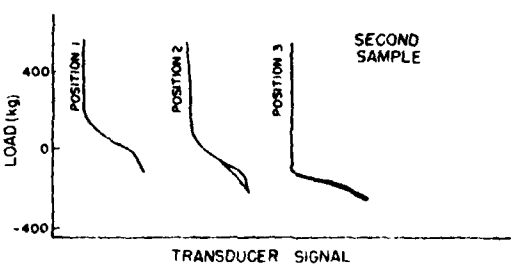

FIG.5
Experimental Measurement of P_{open}, P_B and P_C

Appendix D

Fatigue Crack Closure and Residual Displacement Measurements on Aluminum Alloys

Deepak S. Mahulikar and H.L. Marcus
Mechanical Engineering and
Materials Science and Engineering
The University of Texas
Austin, Texas 78712

Introduction

During fatigue crack growth, plastic deformation is left in the wake of the crack. As a result of this residual deformation, the crack can physically close during the lower part of the tensile crack unloading. This closure phenomenon has been observed and studied extensively[1-10]. Various measurement techniques have been employed to measure crack closure, and many interesting observations are presented on the basis of those measurements. With the help of potential drop measurements Lindley and Richards[5] concluded that crack closure is only a surface or edge effect. Potential drop measurements have been used by other researchers[9,10]. Irving[9] did experiments in vacuum as well as humid air and observed crack closure only in vacuum. Bachman and Munz[10] however, found that closure is present in vacuum as well as at 760 Torr pressure and that the crack opening stress intensity (K_{op}) was independent of environment.[12] A very important conclusion of their

study was that in humid air environment, an oxide layer develops on the crack surfaces, and this effect might give some erroneous results in terms of the potential drop measurements. They point out that earlier results based on the potential drop measurements can be reinterpreted.

Mahulikar et al[7] have discussed edge effects on crack closure. Because of the plane stress region at the edges of the compact tension specimen, surface measurements are not representative of the bulk behavior. Ultrasonic bulk measurements have demonstrated that crack closure is a plane strain as well as a plane stress effect[7,3]

Studies of the residual displacements left in the wake of the crack, can give some important information about crack closure. The residual displacement is considered to be made up of the nonuniform plastic strain on the surface, the small change in volume due to the deformation process and the oxide formed on the nonuniformly strained fracture surface. It was demonstrated[11] that the residual displacements can be measured by a clip on gage mounted on the side of the specimen. Sewell and Marcus[11] measured the residual displacements, (d), for different specimens in humid air and proposed a finite element model to predict crack opening load (P_{op}) using the 'd' measurement.

In order to clearly define the relationship of d with P_{op}, it was necessary to perform experiments in vacuum as well

as other environments. Contributions of plane stress region and oxidation to the residual displacement must be studied. This paper presents the results for such experiments on aluminum alloys. An effort has been made in this paper to relate ultrasonic bulk measurements of crack closure to the surface measurements of the residual displacement. The results clearly demonstrated that surface measurements have limitations and use of such surface measurements for predicting certain aspects of fatigue crack growth can be misleading.

Experimental Procedure

Experiments were performed on the 7075-T651 and 2219-T851 aluminum alloys. Compact tension specimens with dimensions B = 2.54 cm (thickness), H = 5.3 cm (halfheight) and W = 10.8 cm (width) were used. Four types of experiments were performed.

In a first set of experiments only one type of environment (e.g. vacuum) was used. The crack was initiated and grown in that environment at constant ΔK. Closure curves were obtained by ultrasonic techniques described elsewhere[3]. Residual displacements were measured by a clip on gage mounted on the side of the specimen. Since the legs of the clip on gage are approximately 7 mm in length, it was necessary to take two readings to determine the residual displacement d. The initial reading (Fig. 2) was taken just before crack entered the gage and the final reading was taken just after the crack left the gage. The technique to obtain d value is described in [11]. The

geometry of the combined measurement is shown in Fig 1. The gages were mounted at a/w = 0.48.

In another set of experiments the crack was first grown in vacuum and the 'd' measurement curve was obtained by the gage mounted at a/w = 0.48. The cycling was then stopped and the specimen held at the mean load (P_{mean}). D_2O water environment ($\cong$100% RH) was then introduced. As soon as the D_2O water was introduced the residual displacement, d , was obtained. Cycling was then continued at constant ΔK, and after 1000 cycles the d measurement was repeated.

In the third set of experiments, the crack was grown in vacuum, but before introducing D_2O water, dry nitrogen gas was introduced and the d curve was obtained. D_2O water was then introduced and d measurement repeated. The fourth type of experiment on the 7075 alloy consisted of introducing dry O_2 gas after the introduction of N_2 gas.

For ultrasonic measurements, two 2.25 MHz longitudinal transducers of 12.7 cm dia. were used. All the experiments were done in an all metal, ion pumped, environment chamber mounted on an MTS electrohydraulic testing machine. The frequency of cycling during fatigue crack growth was 6 Hz. The ultrasonic and d measurements were made at .06 Hz. Loading parameters for each experiment are presented with the results.

Results

Fig. 2 and 3 show typical ultrasonic transmission curves

as a function of applied load for closure measurement and d measurements respectively. In Fig. 1, P_1 represents the load at which the curve deviates from linearity, while P_2 represents the closure load obtained from the tangent method[3]. In Fig. 2 the initial d displacement curve represents the reading taken before the crack enters the gage and the final curve represents the reading taken just after the crack leaves the gage. The x-axis shift represents 2 d units since d is defined as the residual displacement on one fracture surface.

Fig. 4 shows the effect of environments on the closure load (P_2) and on the d values observed for 7075-T651 alloys. Fig. 5 shows the same effect for the 2219-T851 specimens. Fig. 6 plots the crack growth rates against the effective stress intensity ΔK_{eff} as calculated from P_2 for both the alloys.

The d curves presented in Fig. 7 are for the four types of experiments defined in the experimental procedure section. Fig. 7 (a) is representative of the first type of experiment; Fig. 7 (b) represents the third type of experiment and Fig. 7 (c) represents the fourth type of experiment.

Discussion

The following observations can be made from Figs. 3 and 4.

a) The closure load appears to decrease with increase in humidity. It also decreases as the d value increases.

b) The value of d increases with the introduction of humidity.

c) The values of d for the higher strength 7075-T651 alloy

are higher than the 2219-T851 alloy; and so are the closure loads.

Thus, it was observed that the closure load bears an inverse relationship with the d values. This unexpected result can be explained by the fact that d measurement is a surface measurement and ultrasonic measurement of closure is a bulk measurement. It should be noted that the ultrasonic transducers of 1.27 cm dia. were mounted on a specimen 2.54 cm thick at the middle portion. Thus they were sampling a columnar region of approximately 1.27 cm dia. in the center of the specimen. The plane stress edge region of the specimen was not being sampled. On the edges, the residual displacement was higher than the region sampled by the transducers. Thus even though closure occurred first on the edges, the ultrasonics would not detect it until the inner portion and largest portion of the crack front was compressed sufficiently to touch the surfaces. On the other hand, the d measurements shown are a surface measurement representative of the plane stress plastic deformation at a distance behind the crack tip. In humid air environment a faster buildup of oxide layer on the surfaces of the crack occurs. This effect can be expected to be more severe on the plane stress surface region of the specimen. The 'extra' material consisting of the oxide layer as well as mechanical strengthening of asperities by the oxide on the edges of the crack front results in

increased d value in humid air beyond that of just the oxide thickness. Therefore during the reverse loading more material is available for contact on the edges of the specimen than in the middle of the specimen. Therefore the crack front in the middle of the sepcimen can only touch after the load is reduced further and a lower closure load is observed on the ultrasonic signal.

For 7075 alloy the 'd value in dry 0_2 gas is lower than for humid air as would be expected due to the slower formation of the oxide layer in dry O_2 gas than in humid air. The crack growth rate is seen to increase with the humidity (Fig. 6) as does the ΔK_{eff} calculated using P_2.

An interesting observation was made during the second set of experiments (Fig. 7a). The crack was grown through the clip on gage in vacuum and the d curve was obtained as usual. The cycling was then stopped and the specimen was held at the mean load. D_2O water vapor to 100% RH was then introduced in the environment chamber. As soon as the water vapor was introduced, the gage recorded a shift (Fig. 7a) in the displacement reading. This shift was of the order of 3 to 10 μm for the 7075 alloys. The shift increased slowly with time. After about an hour it was about 12 μm. After this cycling was continued for 1000 cycles and a d curve was recorded with a smaller further increment to the value of d. This shift in d value after the introduction of the D_2O water vapor is most likely due to the formation

of oxide layer which gives mechanical strengthening of the asperities on the edge of the specimen. However, the magnitude of this shift is certainly not representative of oxide layer thickness on aluminum surfaces which leads one to believe that some additional mechanisms associated with the oxide formation must be operating. The strengthening of the asperities is a possible mechanism.

In order to establish that the change in pressure in the system was not the cause of the d shift, the third set of experiments were carried out. After the crack was grown in vacuum but before introducing D_2O water, dry N_2 gas was introduced (Fig. 7b). This showed no change or shift in 'd' reading. This eliminated the possibility of a strictly mechanical effect from the pressure change to explain the change in d. D_2O water was then introduced, which again showed a significant shift in the d value that increased even further on subsequent cycling.

The experiment was then repeated with dry O_2 gas introduced after the vacuum and N_2. The shift in d was very small ~1 μm and further cycling in the dry O_2 showed only a small increase in d value, Fig. 7c.

Thus it was concluded that oxidation played a dominant role in this shift. Oxidation in a dry O_2 gas environment is a very slow process when compared to oxidation in a humid environment. This fast oxidation in a humid environment must attack the plane stress surface portion of the crack

preferentially. This results in changes in the residual displacement probably due to mechanical strengthening by the oxides of asperities that are more dominant on the edge of the specimen. These effects yield the shift in d readings, while the edge effect holding the crack open results in a lower closure load in the center.

It was thus apparent that a lot of changes on the edges or surfaces of the crack front take place when one goes from vacuum to humid air. Surface readings can be entirely different than the bulk readings because of effects of oxidation, such as the strengthening of asperities. Surface clip on gage measurements, thus, cannot be considered totally representative of the bulk closure behavior. Thus the use of d surface measurement for load predictions in a varying environment must be carefully evaluated. In fact using the data presented here, the d measurements combined with a finite element analysis would predict a higher crack closure load, a lower ΔK_{eff} and reduced growth which is contradictory to experimental observations.

Conclusions

1. In 7075-T651 and 2219-T851 the closure load decreased with the introduction of humid environments for both the alloys, while residual displacement d values increased,
2. The decrease in the closure load with humidity is attributed to buildup of extra material at the edges of the specimen which the acoustic transducers do not sample.

3. The increase in d value when fatigued in humid environment compared to vacuum is attributed to the buildup of oxides on the edges of the fracture surface.
4. The d value was observed to increase when D_2O water environment was introduced after the crack was grown in vacuum. Dry O_2 gas introduced after crack growth in vacuum showed only a very small shift in d value.
5. The shift in d value resulting from the introduction of D_2O water vapor after the crack was grown in vacuum was found to increase with time and additional cycling.
6. It is suggested that in addition to oxide formation itself, preferential strengthening of asperities at the edge of the specimen may explain the increase in d in humid air environments.
7. Surface measurements are not always representative of the bulk behavior and use of such measurements in predictive analysis can be misleading.

Acknowledgement

This research was supported by the AFOSR, under contract no. 76-2955. Experimental assistance given by Norman Williams, Anna Zurek and Carlos Arias is highly appreciated.

References

1. Elber, ASTM STP 486, 230 (1971).
2. Schive, Eng. Fract. Mech. V11 pp. 167-221 (1979).
3. Buck, Ho, Marcus. Eng. Fract. Mech. 5, 23 (1973).
4. Sharpe, Corbley, Grandt. ASTM STP 595, 61 (1976).
5. Lindley and Richards, Mat. Sci. Eng. 14, 281, (1974).
6. McEviley, "Current Aspects of Fatigue," presented at the "Fatigue 1977 Conference" University of Cambridge, England (March 28-30, 1977).
7. Mahulikar, Slagle and Marcus, Scripta Met. 13, 867 (1979).
8. Bachman and Munz. Int. J. Fract. 11, 713 (1975).
9. Irwing, Robinson, Beevers. Int. J. Fract 9, 264-282 (1973).
10. Bachman and Munz. Eng. Fract. Mech. 11, 61-71 (1979).
11. Sewell and Marcus, Scripta Met. 11, 521 (1977).
12. Bachman and Munz. Int. J. of Fracture 11, 713 (1975).

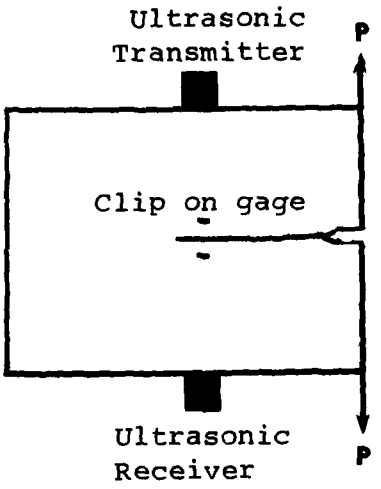
Ultrasonic
Transmitter
P
Clip on gage
Ultrasonic
Receiver
P

Fig. 1

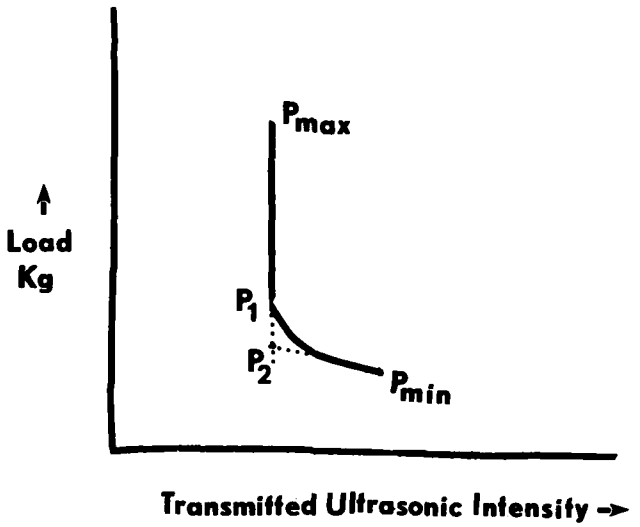
Load
Kg
P_{max}
P_1
P_2
P_{min}
Transmitted Ultrasonic Intensity →

Fig. 2

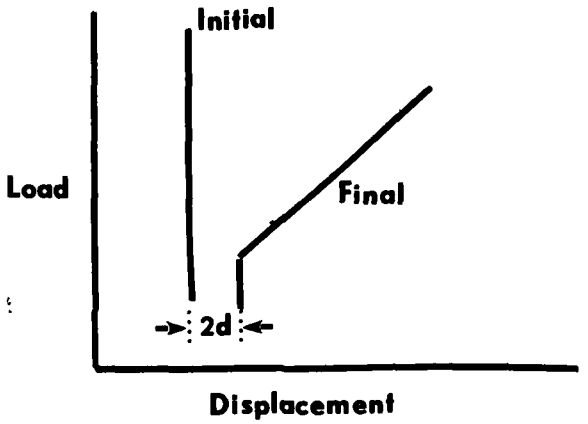
Initial
Load
Final
2d
Displacement

Fig. 3

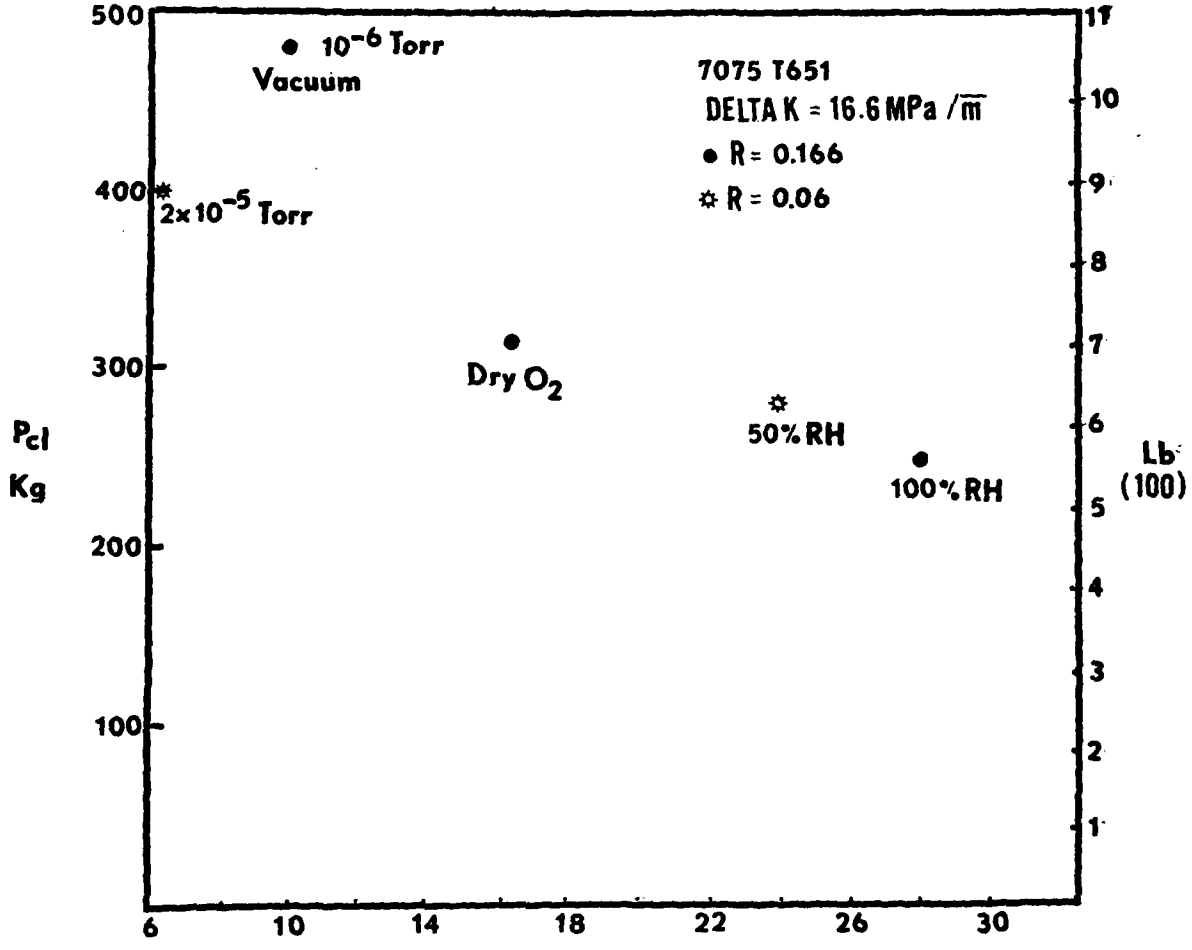

Closure Load Vs Residual Strain Parameter

Fig. 4

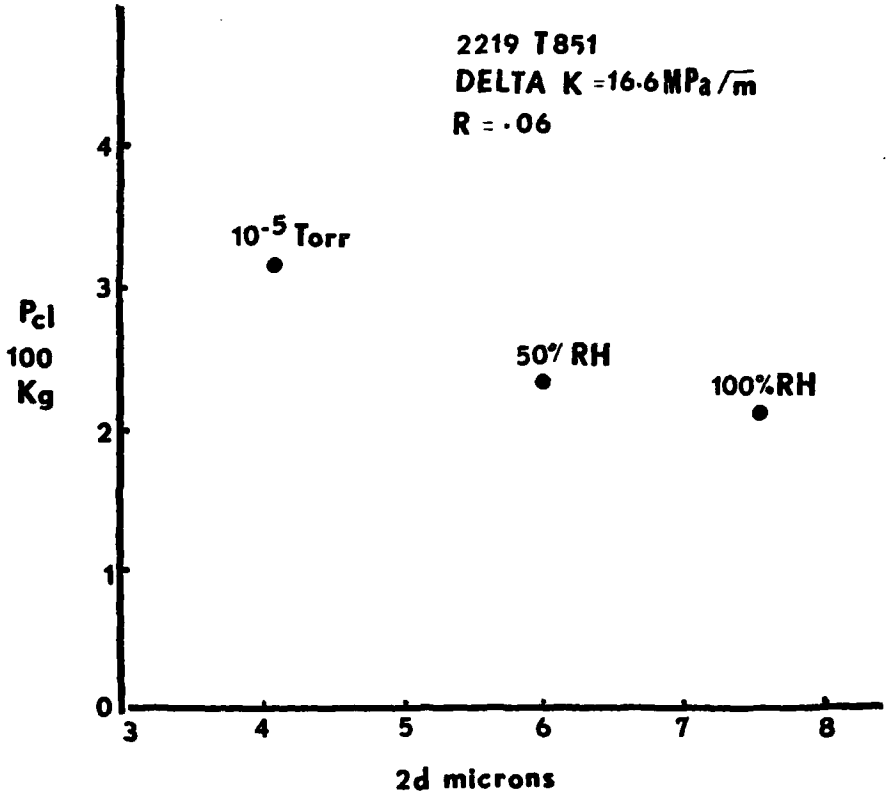
2219 T851
DELTA K =16.6MPa/m
R = .06
10-5 Torr
50% RH
100%RH
Pcl
100
Kg
0
1
2
3
4
3
4
5
6
7
8
2d microns

Fig. 5

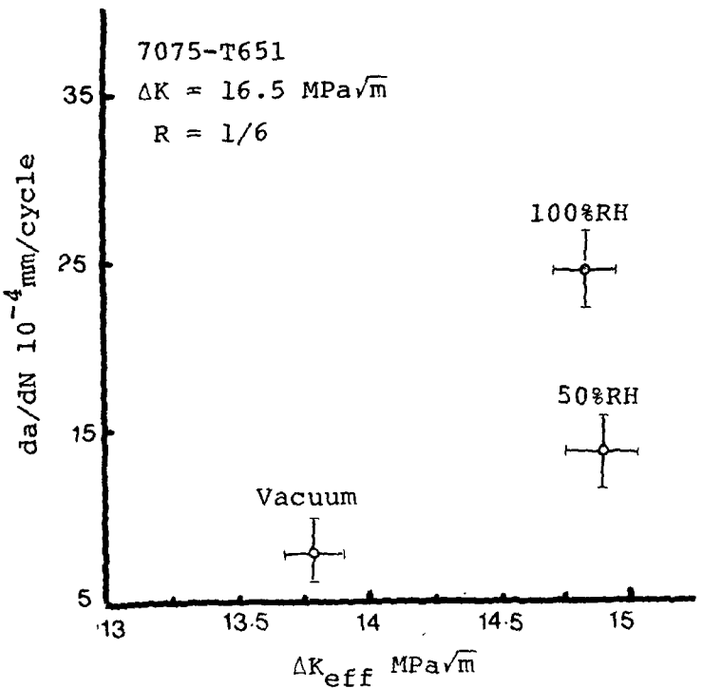
7075-T651
ΔK = 16.5 MPa√m
R = 1/6
100%RH
50%RH
Vacuum
35
25
15
5
13
13.5
14
14.5
15
da/dN 10⁻⁴ mm/cycle
ΔK_eff MPa√m

Fig. 6a

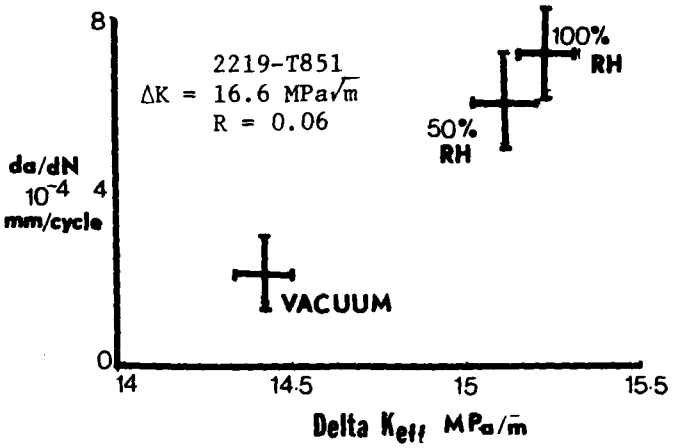
8
2219-T851
ΔK = 16.6 MPa√m
R = 0.06
100%
RH
50%
RH
da/dN
10^-4 4
mm/cycle
VACUUM
0
14
14.5
15
15.5
Delta K_eff MPa√m

Fig. 6b

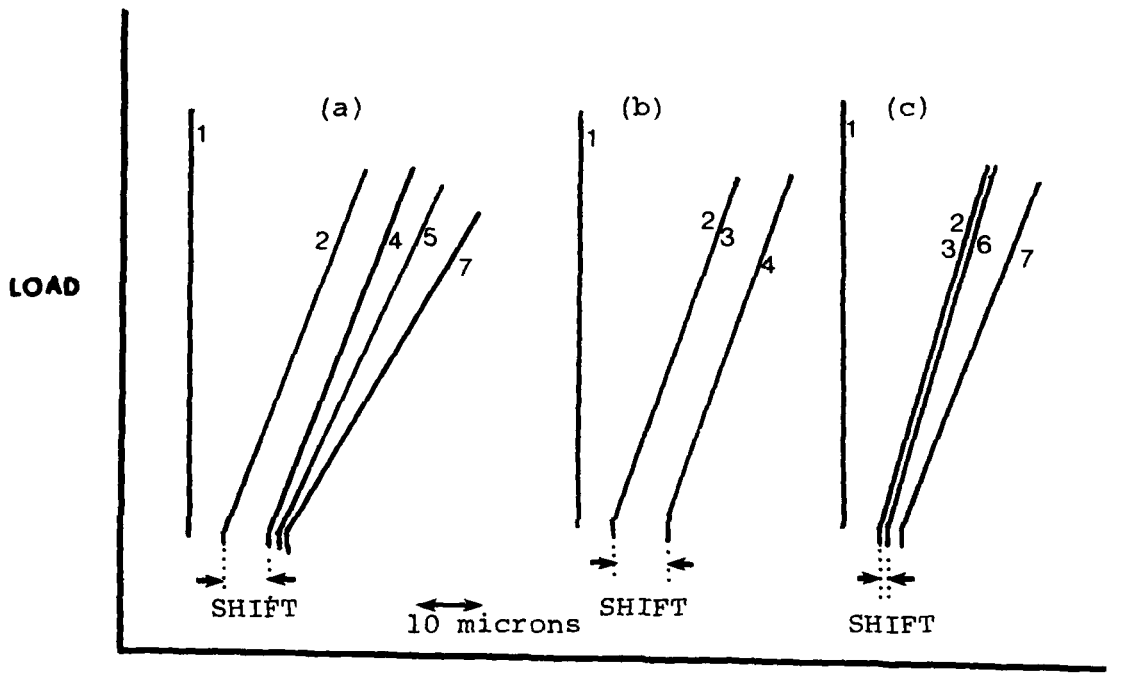

Fig. 7: 'd' measurements in different environments.
1: Initial in vacuum 2: Final in vacuum
3: Introduction of nitrogen gas at-.2 MPa
4: Introduction of D_2O water at -.18 MPa
5: 1 hour after
6: Introduction of dry oxygen gas at-.18MPa
7: After 1000 cycles at constant delta K

Scripta METALLURGICA Vol. 13, pp. 867-870, 1979 Pergamon Press Ltd.
Printed in the U.S.A.

Appendix E

EDGE EFFECTS ON FATIGUE CRACK CLOSURE OF ALUMINIUM ALLOYS

D.S. Mahulikar, W.P. Slagle* and H.L. Marcus
Mechanical Engineering/Materials Science and Engineering
University of Texas, Austin, Texas 78712

(Received June 18, 1979)

Introduction

The crack closure effect suggested by Elber (1) has been studied quite extensively. The fact that the crack closes in the lower part of load cycle has been observed and measured universally but the extent to which the closure affects retardation phenomenon is not yet known clearly. There have been speculations that the crack closure effect is only a surface or edge effect. This was supported by experiments of Lindley and Richards (2). They used potential drop measurements as well as metallographic techniques to study closure effects in the steels. They concluded that crack closure is only a surface or edge effect. This possibility is also discussed by other researchers (3,4). It was suggested that the crack closes only at the surface or edges of the specimen where plane stress conditions exist, while it may not close in the central part where plane strain conditions exist. This paper reports on experiments aimed at clarifying this point.

Experimental Procedures

Several experiments were performed to study this edge effect. Experiments were done on 7075-T651, 2219-T851 and overaged 2219 aluminium alloys. The mechanical properties of these materials are listed in Table 1. Compact tension specimen with dimensions B=2.54 cm thick, H=5.3 cm halfheight and W=10.8 cm long were used.

Two types of experiments were performed on the 7075-T651, 2.54 cm thick specimens. In the first set, the crack was grown up to 4.31 cm at a constant ΔK (16.5 MPa$\sqrt{m}$) and the load ratio, R=0.17, on a closed loop hydraulic testing machine. Closure measurement was made by two 1.27 cm diameter ultrasonic transducers mounted directly above and below the crack tip and centered on the width of the specimen. The ultrasonic technique of load and crack length measurement is described elsewhere (6). In our experiments, the ultrasonic wavelength was significantly longer than the crack tip radius, hence the possibility of closure curve changes being only diffraction or scattering effects was considered unlikely. The experiment was then stopped and two sides of the specimen were machined down to a thickness of 1.75 cm. Again the closure readings were taken at the same point. The cycling was resumed at the same ΔK value and the crack was grown to about 4.8 cm and closure reading were taken directly above the crack tip. The same procedure was repeated by machining down the specimen to a thickness of 1.25 cm, taking closure measurement at that point, and again after growing the crack to a length of 6.3 cm. The results are presented in Fig. 1 where the applied stress intensity is plotted against the received acoustic intensity.

---

* Present address: Celanese Corporation, Corpus Christi, Texas.

0036-9748/79/090867-04$02.00/0

In a second set of experiments a specimen used for relaxation experiments (5) was used for edge effect experiments. A fatigue crack was grown in a 7075-T651 specimen to a length of 4.84 cm at a ΔK of 6.6 MPa$\sqrt{m}$, R=0.33. It was allowed to rest at a zero load for a period of 77 hours for relaxation measurements. Closure measurements were made at the end of the zero load hold time. Then the specimen was machined down to a thickness of 1.3 cm, thus insuring that entire plane stress region was removed. Closure measurements were made at this point. Cycling was resumed and the crack was grown to around 5.4 cm length with continual measurement of closure.

Similar tests were performed on 2219-T851 and overaged 2219 alloys. In these tests the crack was grown at a frequency of 2 Hz, ΔK=26.4 MPa$\sqrt{m}$, and R=0 to a length of 5.6 cm. At this point cycling was stopped and closure measurements were made. Both sides of specimen were then machined off to a thickness of 1.9 cm and closure was measured with the transducers at same position over the crack tip. The specimen was then machined off from both sides to a thickness of 1.3 cm and once more closure measurements were made.

It should be noted that the original specimen thickness was 2.54 cm, twice the diameter of the 1.27 cm ultrasonic transducers. The ultrasonic signal outside this 1.27 cm columnar region does not contribute significantly to the amplitude of the output because of the method used in converting the signal in the peak to peak detector. At a specimen thickness of 2.54 cm the signal transmitted through the plane stress region does not contribute significantly to the output signal intensity since the transducers are centered across the thickness of the specimen.

Results and Discussion

Closure curves are presented in Fig. 1. Two stress intensities K_1 and K_2 were obtained from the curves. K_1 is the intensity at which the closure curve deviates from linearity while K_2 is the closure intensity determined by the tangent method described by Buck et al. (6). Tables 2, 3, 4 and 5 list all the values.

From the ultrasonic measurements for both the alloys and all cases, significant crack closure was still observed after machining off the plane stress region as is evident from Fig. 1 and Tables 2, 3, 4 and 5.

For 7075 alloys, it was observed that machining off the sides did not change the closure stress intensities significantly. However, as the crack was grown further, the values of K_1 and K_2 increased. On the other hand for 2219 alloys a significant increase in K_1 and K_2 was observed after machining off the sides.

These observations can be explained from the fact that 7075 is a high-strength, low K_{1c} alloy. Hence the plastic zone sizes encountered are relatively smaller. Thus within the limits of ultrasonic measurements K_1, K_2 did not change significantly. When the crack was grown further, new plane stress region developed indicating slight rise in K_1 and K_2 at a thickness of 1.75 cm and a significant rise at a thickness of 1.25 cm. The significant rise can be understood by the fact that the thickness is very small, slightly greater than allowable thickness for plane strain testing, and transducers are now sampling the entire thickness of the specimen. Higher ΔK values were not used due to the limitations of the fracture toughness.

For 2219 alloys, machining off the sides of the specimens instantaneously increased the values of K_1 and K_2. 2219 has a lower σ_y and higher K_{1c} than 7075. The higher K_{1c} made it possible to use higher ΔK values for the experiment. This combined with the lower value of σ_y makes the plastic zone sizes significantly larger. When the specimen was at the original thickness this large plastic strain in the plane stress region allowed the specimen edges to close before the plane strain region. This served to prop open the interior and keep it from closing until the load was reduced enough to sufficiently compress the plane stress region so the interior closed. The result was a lower closure stress intensity detected by ultrasonics. Once the

plane stress region was machined off the remaining plane strain region would close at a higher value of K.

A brief mention should be made of the residual stresses. Residual stresses are introduced on the surface of the specimens because of heat treatments given to them and also because of machining. The extent to which these stresses can affect the closure behaviour is not yet well understood, but are not expected to be significant in these experiments.

Conclusions

1. Significant crack closure was observed for ultrasonic measurements made after machining off the plane stress region of the fatigue crack in 7075 and 2219 aluminium alloys.

2. For high strength low K_{1c} 7075 alloys closure stress intensities did not change significantly after machining off the sides of the compact tension specimen, however K_1 and K_2 increased after the crack was grown further.

3. For relatively low strength high K_{1c} 2219 alloys the value of K_1 and K_2 increased after machining off the sides. This is attributed to relatively large plastic zone sizes in 2219.

4. Crack closure is not only associated with the edge of the specimen, but with the total crack front in compact tension specimens.

Acknowledgement

This research was supported by the Air Force Office of Scientific Research, NE Contract Number 76-2955.

References

1. W. Elber, ASTM STP 486, 230 (1971).
2. T.C. Lindley and C.E. Richards, Mat. Sci. Eng., 14, 281.
3. A.J. McEvily, "Current Aspects of Fatigue," Presented at the "Fatigue 1977 Conference" Univ. of Cambridge, England (March 28-30, 1977).
4. T.T. Shih, and R.P. Wei, "A Study of Crack Closure in Fatigue," NASA CR-2319 (1973).
5. Slagle, W.P., M.S. Thesis at the Univ. of Texas at Austin (May, 1979).
6. O. Buck, C.L. Ho, H.L. Marcus, Eng. Fract. Mechanics, 5. 23 (1973).

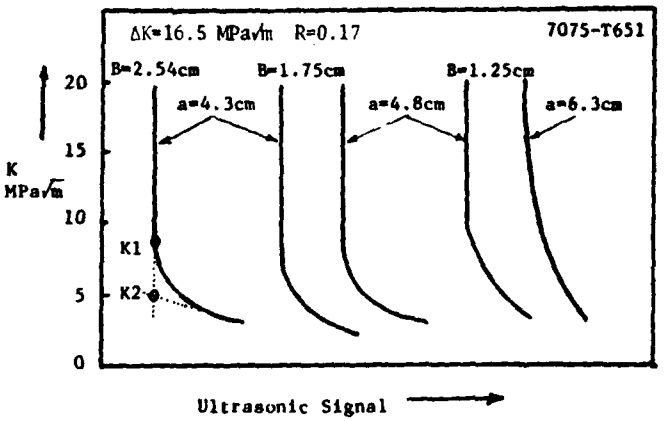

FIG.1
Closure Curves for 7075-T651 Alloy for Different Thicknesses of the Compact Tension Specimen.

TABLE 1

Yield Strengths and K_{1c} Values of Specimen Materials

Material	σ_y MPa	K_{1c} MPa$\sqrt{m}$
7075-T651	505	25
2219-T851	350	35
2219-overaged	200	36

TABLE 2

Material: 7075-T651; ΔK=16.5 MPa$\sqrt{m}$

Thickness B (cm)	Crack Length a (cm)	K_1 (MPa$\sqrt{m}$)	K_2 (MPa$\sqrt{m}$)
2.54	4.3	8.3	5.005
1.75	4.3	7.3	4.334
1.75	4.8	8.2	5.225
1.25	4.8	8.35	4.455
1.25	6.3	16.8	8.36

TABLE 3

Material: 7075 T651; ΔK=6.6 MPa$\sqrt{m}$

B (cm)	a (cm)	K_1 (MPa$\sqrt{m}$)	K_2 (MPa$\sqrt{m}$)
2.5	4.8	2.43	1.73
1.3	4.8	3.31	1.56
1.3	5.4	3.34	1.95

TABLE 4

Material: 2129-T851; ΔK=26.4 MPa$\sqrt{m}$

B (cm)	a (cm)	K_1 (MPa$\sqrt{m}$)	K_2 (MPa$\sqrt{m}$)
2.5	5.6	7.6	4.6
1.9	5.6	15.6	5.1
1.3	5.6	10.8	6.6

TABLE 5

Material: Overaged 2219; ΔK=26.4 MPa$\sqrt{m}$

B (cm)	a (cm)	K_1 (Mpa$\sqrt{m}$)	K_2 (MPa$\sqrt{m}$)
2.5	5.6	8.2	3.1
1.9	5.6	15.6	8.8
1.3	5.6	11.8	5.1

Appendix F

THE INFLUENCE OF FATIGUE CRACK SURFACE ROUGHNESS ON ACOUSTIC WAVE TRANSMISSION

John A. Jeffries* and H.L. Marcus
Mechanical Engineering/Materials Science
The University of Texas at Austin
Austin, Texas 78712

O. Buck
Fracture and Metal Physics Group
Rockwell Science Center
Thousand Oaks, California

Abstract

This paper is concerned with the measurements that simulate the amplitude of acoustic waves transmitted through a simulated crack interface as the compressional load on the crack is varied and as the roughness of the crack is varied. The samples either have specific roughness mechanically produced or are cut from compact tension specimen run at different stress intensity ranges and in different environments that represent actual fatigue crack surfaces. Using an electro-hydraulic testing machine, two aluminum blocks are loaded in compression until the maximum acoustic transmission is observed. It is observed that the amplitude of acoustic wave transmitted through the interface reaches the maximum at different stress levels depending on the interfacial surface roughness. Additional variables of the study are the frequency of the acoustic waves, and the relative humidity both during the fatigue test and during the acoustic evaluation. A model is described showing the correlations between load, surface roughness, acoustic frequency, and environment on the transmitted energy. The results are then related back to the extent of crack closure observed acoustically on a fatigue cracked specimen.

A. INTRODUCTION

This paper is concerned with the measurement of the attenuation of longitudinal acoustic waves as they are transmitted through a simulated fatigue crack interface in Al 2219 and Al 2024 alloys. Additionally, combining the acoustic data with an elastic finite element analysis that defines the stress distribution across the interface it is shown that it is, in principle, possible to determine the actual extent of crack closure from acoustic data taken during the fatigue cycle. The variables of this study are the ap-

*Currently employed as a Staff Engineer at Texas Instruments, Austin, Texas.

Published in Proceedings of 11th Symposium on NDE, ASNT and SRI, San Antonio, Texas 275 (April 20-22, 1977).

plied load, surface roughness of the simulated fatigue crack interface, and frequency of the acoustic waves.

B. SPECIMEN PREPARATION

The aluminum blocks were cut from plate stock and parallel ground to minimize any effects of rocking action between the surfaces. After being ground, the blocks were metallurgically polished on the surfaces that were to serve as the simulated interface. Next, the polished surfaces were grit blasted with varying grits to produce the desired variations in surface roughness. The 400 microinch(RMS) sample was cut from an actual fatigue crack grown in a compact tension specimen. The authors feel grit blasted surfaces closely approximate the nature of a real fatigue crack surface where tearing and hammering have occurred, thus preventing any matching of the surfaces on a microscopic scale (Fig.1).

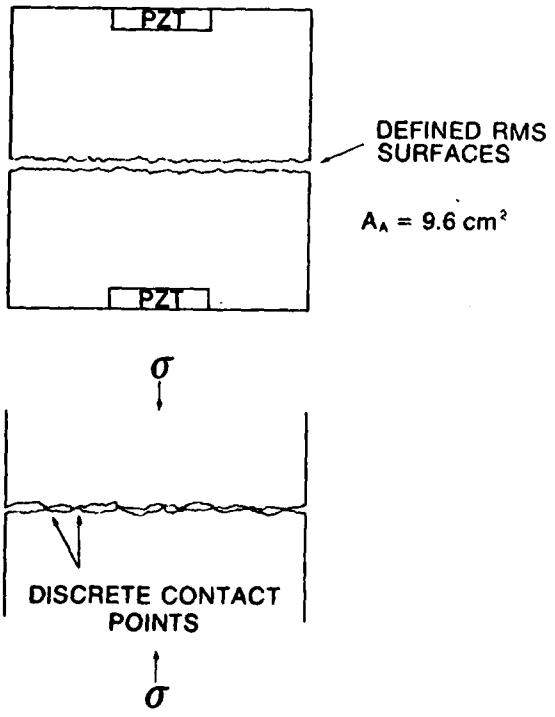

FIGURE 1. THE SIMULATED FATIGUE CRACK

The Al 2024 specimens had the model surfaces machined to achieve the desired roughnesses, with the exception of the 4 microinch sample which was grit blasted. The machining led to a much coarser roughness than the grit blasting.

C. EXPERIMENTAL TECHNIQUE

The blocks were placed in an MTS closed-loop electrohydraulic testing machine and the upper and lower mandrels were slotted so the longitudinal wave acoustic transducers could be placed directly on the blocks. The interface between the transducers and the blocks was of silicone based grease. Compression springs were used to hold the transducers firmly against the blocks. The acoustic signal was generated by a standard pulse oscillator, travelled from the input transducer through the simulated fatigue crack to the output transducer, then to an AC-DC converter, and finally to an X-Y plotter where it appeared on the ordinate axis. The load signal was taken directly from the MTS controller and appeared on the abscissa axis. Thus the outputs of the experiment could be directly plotted while the system was cycling (at 0.03 Hz.) Typically about fifteen cycles were required for the output signal to stabilize and the data reported is from after stabilization of the signal had occurred. The loading cycles were from zero compressional load to a compressive load of approximately 30 percent of the yield strength of the material, based on the apparent area of contact. To seperate out the transducer coupling effect a block with no interface was used.

D. EXPERIMENTAL RESULTS

In figure 2 the appearance of a typical fatigue crack is shown. Note that part of the crack is open and part closed consistent with the fatigue crack closure model (1,2) Typically acoustic techniques are used to discover cracks such as this. Previously it has been impossible to determine the size of a fatigue crack from acoustic data because no information was available to determine the amount of acoustic wave transmitted[3] through the closed portion of the crack with crack topography as a variable. Figures 3 and 4 show the dramatic effect of interfacial surface roughness on the amplitude of acoustic wave transmitted through the interface as a function of load. Significantly, the difference in transmission between the grit blasted and machined surfaces for equivalent loading should also be noted. An interesting aspect of the results from the grit blasted specimens is what appears to be a saturation effect (Fig.5), however, the authors feel further investigation will be necessary to verify this finding. Another variable of this study was frequency of the acoustic waves. Comparison of data taken for two dif-

ferent model cracks shows essentially no difference(Fig. 6).

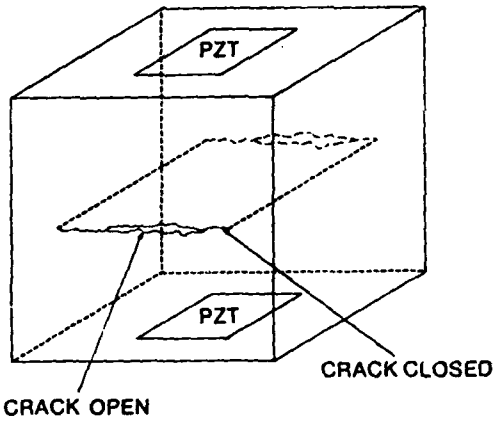

FIGURE 2. A TYPICAL FATIGE CRACK

Addionally, note the similarity in the 4 microinch curves in figures 3 and 4.

result reported previously by Lohanic and Lipschultz[4].

E. ELASTIC FINITE ELEMENT ANALYSIS

The authors will now give a brief description of the computer model for crack closure using a finite element program developed by Sewell[5]. Assume that a fatigue crack growth experiment is carried out on a compact tension specimen. As the crack grows, it will leave behind an approximately uniform wake of residual strain, that is, the material in the wake of the crack tip will effectively become thicker because of the surface roughness and volumn change associated with the high tensile strains near the crack tip before seperation. This increase in thickness is modeled [6] as a uniform coating of new material on the crack surfaces. The normal stress distribution across the crack interface is then established as a function of distance from the crack tip. The stress distribution obtained by the analysis is then available to interpret the transmitted acoustic data from a fatigue crack[2].

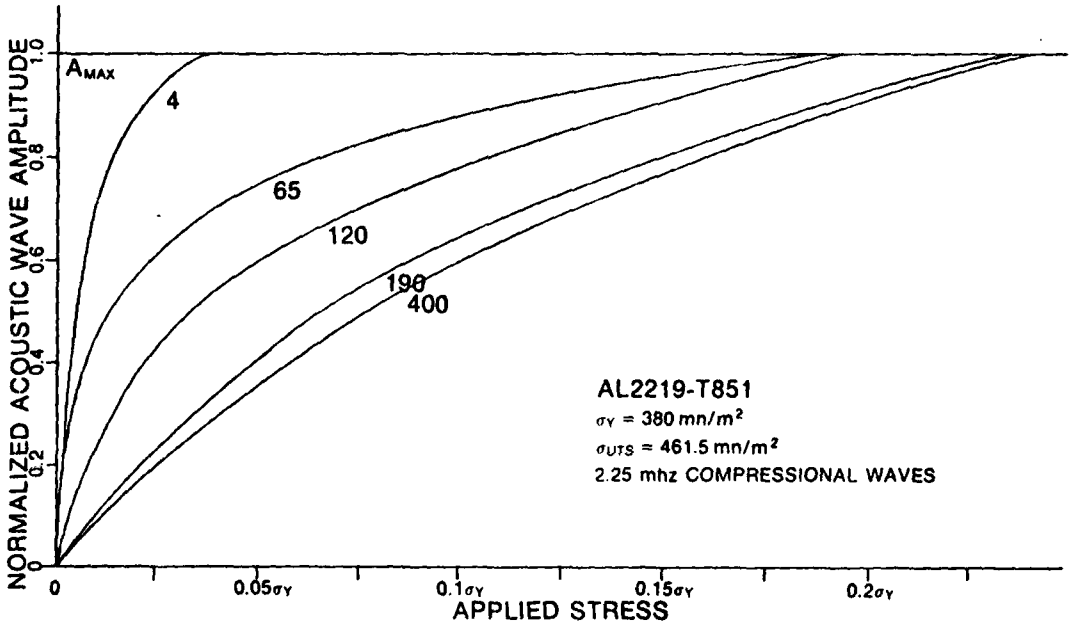

FIGURE 3. ACOUSTIC WAVE AMPLITUDE VS. APPLIED STRESS (GRIT BLASTED SPECIMENS)

The acoustic wave frequencies used here were 2.25 MHz for the former and 1.0 MHz for the latter. Thus the authors feel that there is little frequency effect in the 1.0 MHz to 5.0 MHz regime, a

F. DISCUSSION AND CONCLUSION

The authors have demonstrated that in order to evaluate the true extent of crack closure distance as a function

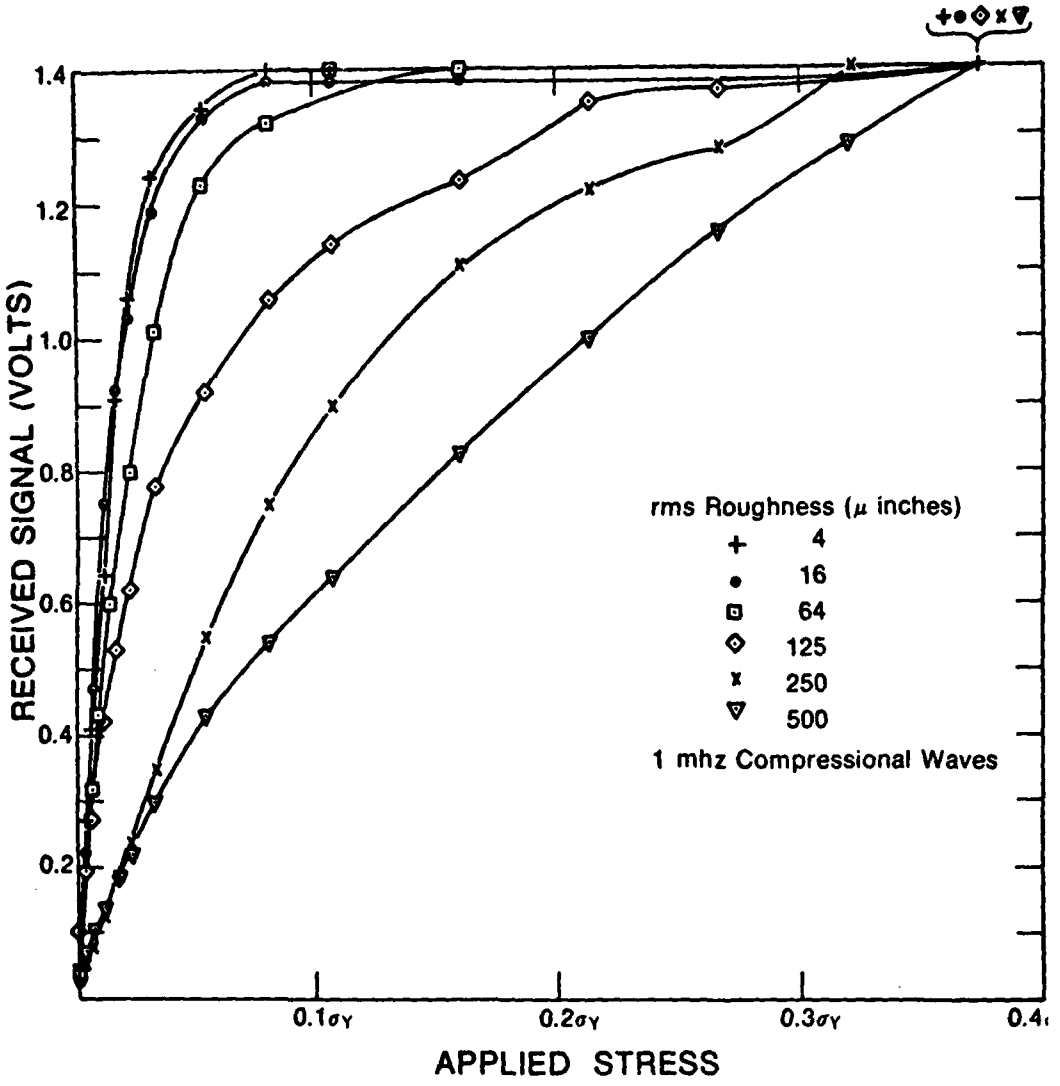

FIGURE 4. ACOUSTIC WAVE AMPLITUDE VS. APPLIED STRESS (MACHINED SPECIMENS)

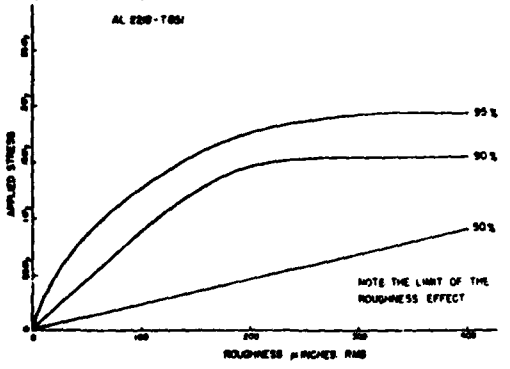

FIGURE 5. THE SATURATION EFFECT

of load it is necessary to consider the compressive stress on the fracture surface, and the transmission factor which is a function of the stress and surface roughness. Using the elastic finite element analysis[6], the extent of closure and the closure stress have been determined allowing the calculation of the acoustic wave transmission across the interface which s given by;

$$T_{AI} = \int_{x=0}^{x=a} T(\sigma(x)RMS)\,dx$$

where T_{AI} = total acoustic transmission across the interface
a = true crack length

x= distance along crack from load line to a.

and,

$T(\sigma(x)RMS)$= the transmission factor as a function of stress and surface roughness

Therefore it is, in principle, possible to predict the amount of transmission due to crack closure from the roughness-stress data presented here combined with the use of the elastic finite element model. It should be noted that the above analysis is for the instantaneous measurement of crack lengths. For NDT purposes the non-elastic behavior of the fatigue crack[7] must be taken into consideration.

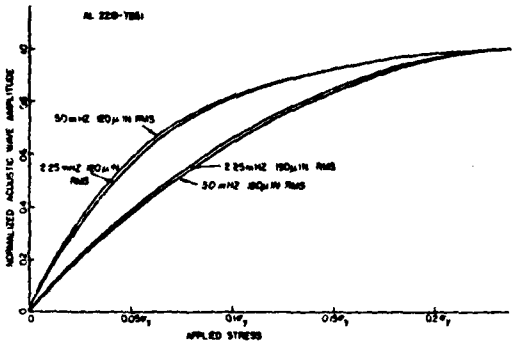

FIGURE 6. THE FREQUENCY EFFECT

Another application of the results of this study is to the choice of load required to acoustically couple a remote sensing transducer through a sensing rod to the structure of interest. In this case the RMS should be minimized to reduce the required loading.

G. ACKNOWLEDGEMENTS

This research was sponsored by the Air Force Office of Scientific Research, Air Force Systems Command, USAF, under Grant No. AFOSR 76-2955. The authors would like to acknowledge the experimental assistance of John Swanson, Carlos Arias, and Dick Inman. Additionally, John A. Jeffries wishes to express his appreciation to Texas Instruments, Inc., Austin, Texas for time allotted to continue this research.

H. REFERENCES

1. Elber, W in DAMAGE TOLERANCE IN AIRCRAFT STRUCTURES, ASTM STP 486,230 (1971).
2. Buck, O.,Ho,C.L., Marcus, H.L.,and Thompson, R.B. in STRESS ANALYSIS AND GROWTH OF CRACKS, ASTM STP 513, 280 (1972)
3. Yee,B.G.W., Couchman, J.C., Hagemeyer, J.W., Chang, F.H. in NON-DESTRUCTIVE TESTING, 245 (1974).
4.Lohanick, A.W., and Lipschultz, F.P. in 1973 ULTRASONICS SYMPOSIUM PROCEEDINGS, 234 (1973).
5. Sewell, G. to be published in TRANSACTIONS ON MATHEMATICAL SOFTWARE.
6. Sewell, G. and Marcus, H.L. to be published in SCRIPTA METALLURGICA, June, 1977.
7. Yee, B.G.W., Hagemeyer, J.W., Chang, F.H., and Couchman, J.C.,"THE EFFECTS OF RELAXATION AND CLOSURE STRESSES ON THE DETECTION OF FATIGUE CRACKS IN 2219-T87 ALUMINUM", General Dynamics Research Report, ERR-FW-1610, 1975.

Appendix G

MODEL FOR ULTRASONIC MEASUREMENT OF TRUE CRACK LENGTH WHEN CRACK CLOSURE EXISTS

John A. Jeffries* and H.L. Marcus**
*Staff Engineer
Texas Instruments
Austin, TX 78750
**Department of Mechanical Engineering
and Materials Science and Engineering
The University of Texas
Austin, TX 78712

MODEL

The amplitude of acoustic wave transmission through the closed portion of a fatigue crack is a function of two variables. These variables are the roughness of the fatigue crack interface and the compressive stress distribution from the point of crack closure to the crack tip. The model to be developed will encompass both of these variables.

In general, the curves described by the plots of acoustic wave transmission versus applied stress (Fig. 4), are roughly approximated by the form:

$$A = A_{max}(1-e^{+n\sigma}) \qquad -1-$$

where A = the amplitude of the transmitted acoustic wave normalized to the maximum transmitted wave

A_{max} = maximum transmitted wave

n = a variable to be determined

and σ = the stress across the interface which is always compressive.

For the roughnesses produced in the compact tension specimens, it was found that the curve described by:

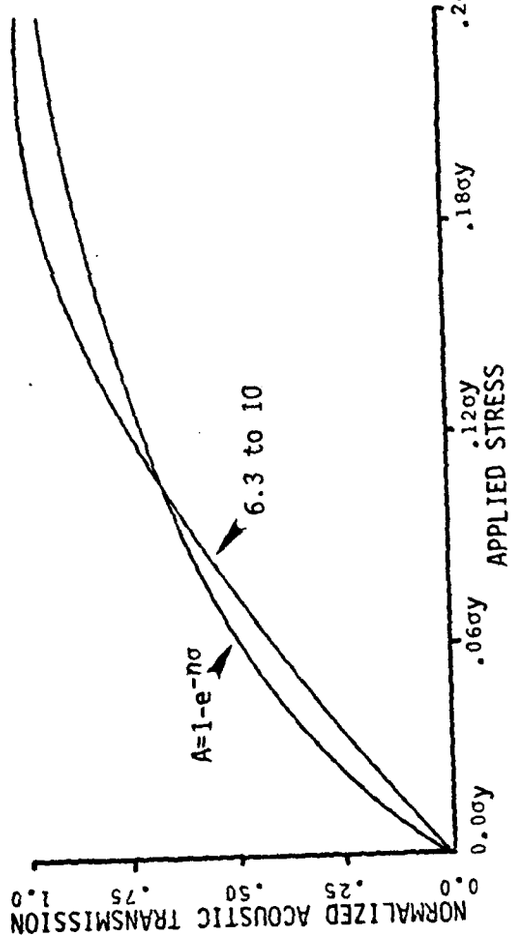

FIGURE 1. ACOUSTIC TRANSMISSION FOR 6.3μ METER RMS TO 10μ METER RMS ROUGHNESS AND FOR $A=1-e^{-n\sigma}$

$$A = A_{max}(1-e^{+.028\sigma}) \qquad -2-$$

closely matches the acoustic wave amplitude versus applied stress curve previously measured (Fig. 10). Here the units of A are arbitrary with a maximum of very nearly A_{max} and σ, the applied stress, is in units of MN/m^2.

If it is assumed that the stress distribution is linear and increases from zero at the point of closure to the yield strength of the material at the crack tip then it is of the form:

$$\sigma = mx \qquad -3-$$

where m is a constant dependent on x, the crack closure distance, and x varies from zero at the crack closure point to x_τ, the distance from the closure point to the crack tip.

The expression:

$$A = A_{max}(1-e^{+mnx}) \qquad -4-$$

describes the predicted transducer output curve. Next, the values of m for the two specimens must be determined. For specimen one:

at $x = 0$, $\sigma = 0$

at $x = x_\tau = .018m$, $\sigma = -380MN/m^2$

$$m = \frac{\sigma}{x_\tau} = \frac{-380}{.018} = -21{,}100MN/m^3$$

For specimen two:

at $x = 0$, $\sigma = 0$

at $x = x_\tau = .005m$, $\sigma = -380MN/m^2$

$$m_2 = \frac{\sigma}{x_\tau} = \frac{-380}{.005} = -76{,}000MN/m^3$$

where the location of $x = 0$ and $x = x_\tau$ have been determined experimentally.

Thus the two equations describing the normalized predicted acoustic wave output for the two specimens are:

$$A_1 = A_{max}(1-e^{+mnx}) = A_{max}(1-e^{+600x}) \qquad -5-$$

and $$A_2 = A_{max}(1-e^{+mnx}) = A_{max}(1-e^{+2150x}) \qquad -6-$$

In order to determine the total normalized acoustic wave transmission across the interface, T_{AI}, the curves must be integrated from x = 0 to $x = x_\tau$, or

$$T_{AI} = A_{max}\int_{x=0}^{x=x_\tau} 1-e^{+mnx}\ dx = A_{max}\ x+\frac{1}{mn}\ e^{+mnx}\ \Big|_{x=0}^{x=x_\tau} \qquad -7-$$

Evaluation of the integral for the two curves yields:

$$T_{AI1} = .0163A_{max}$$

$$T_{AI2} = .0045A_{max}$$

and the units for T_{AI1} and T_{AI2} will be distance times the maximum wave transmission.

In order to determine the percentage of acoustic wave transmission across the interface, T_{AI1} and T_{AI2} must be divided by the integral of the acoustic wave if all transmission began at the closure point, or:

$$T_{AT} = \int_{x=0}^{x=x_\tau} A_{max}dx \qquad -8-$$

where T_{AT} is the total acoustic wave transmission assuming all transmission began at the closure point and A_{max} represents the maximum transmission across the interface. Thus

$$T_{AI1} = \int_{x=0}^{x=x_\tau} A_{max}\ dx = A_{max}\ \Big|_{x=0}^{x=x_\tau} = .018A_{max} \qquad -9-$$

$$T_{AI2} = \int_{x=0}^{x=x_\tau} A_{max}\ dx = A_{max}x\ \Big|_{x=0}^{x=x_\tau} = .005A_{max} \qquad -10-$$

where the units will again be distance times the maximum acoustic wave transmission. Now the transmission percentage, T_{AP}, can be obtained and is equal to

$$T_{AP} = \frac{T_{AI}}{T_{AT}}$$

Therefore

$$T_{AP1} = \frac{.0163A_{max}}{.018A_{max}} = .90 = 90\%$$

$$T_{AP2} = \frac{.0045A_{max}}{.005A_{max}} = .90 = 90\%$$

and the units of the numerator and denominator cancel each other. Thus 10% of the acoustic wave transmission is attenuated by the low stress portion of the crack.

In the preceeding section of the model development it was assumed that the stress distribution from the crack closure point to the crack tip was linear. However, it is better to model the stress distribution as

$$\sigma = mx^2 \qquad \text{-11-}$$

where m is a constant and dependent upon the degress of crack closure. This stress distribution approximates the results of an elastic finite element analysis in Appendix E or that expected from beam theory. The values of m for the nonlinear stress distribution model are obtained in the same manner as for the linear model.

For specimen one:

at $x = 0$, $\sigma = 0$

$$\text{at } x - x_\tau = .018\text{m}, \ \sigma = -380\text{MN/m}^2$$

$$M_1 = \frac{\sigma y}{x_\tau^2} = \frac{-380}{(.018)^2} = -1.17\times10^6\text{MN/m}^4$$

and for specimen two:

$$\text{at } x = 0, \ \sigma = 0$$

$$x = x_\tau = .005\text{m}, \ \sigma = -380\text{MN/m}^2$$

$$M2 = \frac{\sigma y}{x_\tau^2} = \frac{-380}{(.005)^2} = -15.2\times10^6\text{MN/m}^4$$

The model can now be modified to reflect the non-linearity of the stress distribution in the specimens.

For normalized acoustic wave transmission in general the expression is

$$A = A_{max}(1-e^{+mnx^2}) \qquad \text{-12-}$$

where mx^2 has been substituted for σ. The total normalized acoustic wave transmission across the interface becomes

$$T_{AI} = A_{max}\int_{x=0}^{x=x_\tau}(1-e^{+mnx^2})dx \qquad \text{-13-}$$

The evaluation of this integral is in Appendix G1.

Since the value of n has already been determined, the expressions for the normalized acoustic wave transmitted for each specimen are now

$$A_1 = A_{max}(1-e^{-3.33\times10^4x^2}) \qquad \text{-14-}$$

and

$$A_2 = A_{max}(1-e^{-4.31\times10^5x^2}) \qquad \text{-15-}$$

Therefore, the expression for the total normalized acoustic wave transmission across the interface for the two specimens are

$$T_{AI1} = A_{max} \int_{x=0}^{x=.018} (1-e^{-3.33x10^4x^2})dx \qquad -16-$$

and

$$T_{AI2} = A_{max} \int_{x=0}^{x=.005} (1-e^{-4.31x10^5x^2})dx \qquad -17-$$

which, upon evaluation, yield

$$T_{AI1} = 1.31 \times 10^{-2} A_{max}$$

and

$$T_{AI2} = 3.65 \times 10^{-3} A_{max}$$

The units of T_{AI1} and T_{AI2} will again be distance times the maximum acoustic wave transmitted. To obtain the percentage of wave transmission across the interface, the amount of transmission that would occur if all transmission began at the closure point must be determined. This quantity T_{AT}, is equal to that calculated in equations 8 - 10. Now the transmission percentage, T_{AP}, can be determined.

$$T_{AP1} = \frac{T_{AI1}}{T_{AI1}} = \frac{1.31x10^{-2}A}{.018A} = .73 = 73\% \qquad -18-$$

and

$$T_{AP2} = \frac{T_{AI1}}{T_{AI2}} = \frac{3.65x10^{-3}A_{max}}{.005A_{max}} = .73 = 73\% \qquad -19-$$

Therefore, 27% of the acoustic wave transmission is attenuated by the low stress portion of each crack. And it has been shown that the percentage of acoustic wave transmission is independent of the crack closure distance. Note that the percentage transmission obtained is only for the conditions of $\sigma = mnx^2$ stress distribution and a transmission coefficient, A, independent of surface roughness over the range of interest.

DISCUSSION AND APPLICATION OF THE MODEL

It was demonstrated in Appendix C that acoustic wave transmission through a fatigue crack interface is virtually independent of roughness in the 4.8 μmeter to 10 μmeter rms range. In the development of the model in the preceeding section, it was shown that the percentage of acoustic wave transmission through a fatigue crack is independent of closure distance for a fixed stress profile. This independence of closure distance applies to both the linear and quadratic models of the stress distribution normal to the surface along the closure distance. In the prediction of true fatigue crack size the model can be used in several ways.

First of all, it must be noted that when the crack analysis uses measurement of reflected waves rather than transmitted waves, the predicted transmission quantity must be subtracted from one to give the reflected wave quantity.

The two most general cases of crack interrogation occur when the transducers are large relative to the closure distance and when point transducers are used (See Fig. 2).

In the use of transducers large relative to the closure distance two different techniques may be used to account for the crack closure and to predict the crack size. The first of the two techniques requires the use of the predicted percentage of acoustic wave transmission. Since the transducer is large relative to the closure distance the output can be considered the integral of the acoustic wave transmitted

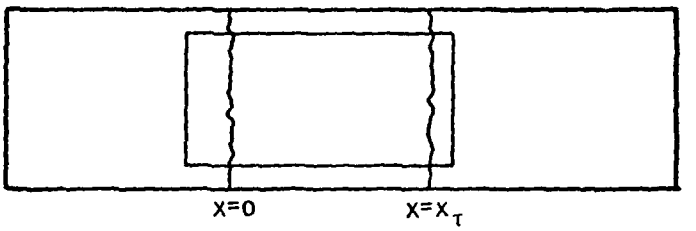

LARGE TRANSDUCER RELATIVE TO CLOSURE

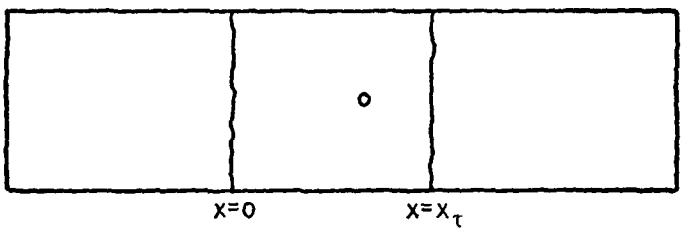

POINT TRANSDUCER

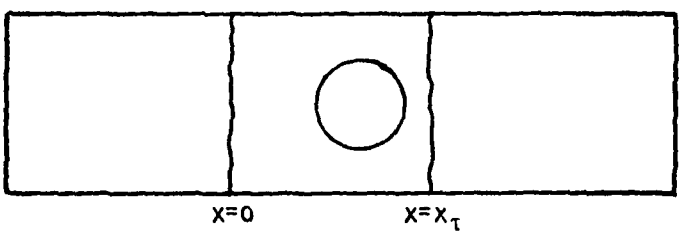

FIGURE 2. THREE TRANSDUCER SIZES RELATIVE TO CRACK CLOSURE DISTANCE

When point transducers are used to examine a fatigue crack, the procedure is essentially the same as that described for the large transducers. Instead of locating the point where the change in output becomes linear, the point where transmission first reaches constant output corresponds to the point, x_c, where the stresses are high enough to make the crack appear transparent to the acoustic waves. Now the distance from the closure point to the crack tip may be determined just as in the preceeding section for large transducers.

When transducers are used in fatigue crack analysis that are smaller than the closure distance, but larger than point transducers and have a non-uniform front, the evaluation becomes more difficult. Now, not only the acoustic wave transmission as a function of stress can be determined, but the geometry of the transducer itself may need to be considered. There are two techniques that may be used with transducers in this size range. The first technique is similar to that developed for large transducers when the predicted percentage of transmission is used. Since the transducers are smaller than the crack closure distance, however, as the transducers are moved along the crack the outputs must be summed. This summation should provide the equivalent of the integral of the acoustic wave output that would be observed if large transducers were used when the geometric effect is taken into account. The technique now is that developed earlier for the large transducers.

The second technique for use with these transducers is essentially the same as the method described for use with the point transducers. The point where transmission begins still corresponds to the crack closure

through the crack. The expected output of the transducer is shown in Fig. 3. At some point along the output curve it becomes linear. This linear portion of the curve corresponds to the increase in transducer area parallel to the crack, past the point where the crack appears transparent to the acoustic waves. If a line is constructed beginning at $x = 0$, the closure point, with the same slope as the linear portion of the output curve, this new curve represents the integral of acoustic wave transmission if complete transmission occurred at the closure point (i.e., it is the integral of A_{max}). Thus, from the model, when the output curve is the predicted percentage of the integral of the A_{max} curve the crack tip has been located. An example of this is shown in Fig. 12.

The second technique for use with the large transducers requires the location of the point along the output curve where the curve first becomes linear. This point corresponds to the point along the crack where transmission is complete. Experimentally, by knowing the point where transmission begins ($x = 0$), the point (x_c) and the stress ($.24\sigma y$) where transmission is 95% complete and assuming the stress at the crack tip (x_τ) is equal to the yield strength of the material, the crack length can be determined. To accomplish this, the assumed stress distribution

$$\sigma = nx^2$$

is used where x is the distance from the closure point to the crack tip. The value of n is then determined by the point where transmission is 95% complete. Then the crack length can be determined from the stress of σy at the crack tip.

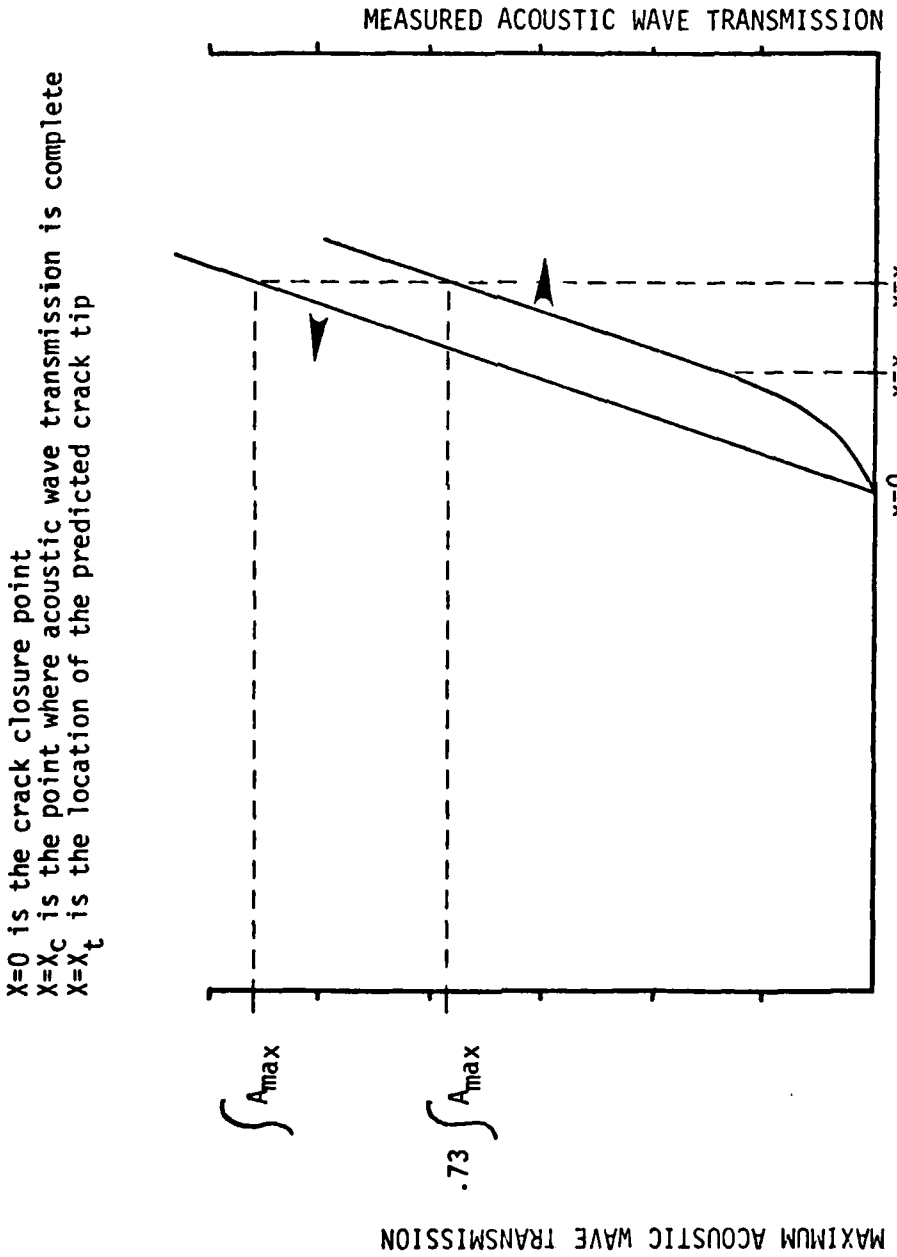

FIGURE 3. TWO METHODS OF CRACK SIZE PREDICTION BASED ON THE USE OF LARGE TRANSDUCERS

point where the compressive stress is zero. To determine the point where acoustic transmission is complete the location of the trailing edge of the transducer must be known. When the acoustic transmission reaches a constant value, the trailing edge of the transducer is at the point, x_c, where transmission is complete. Therefore, as in the case of the point transducers, enough information is known about the crack to predict the true crack length.

A model has now been developed and described which allows the prediction of fatigue crack size in aluminum alloys for three different size transducers relative to the crack closure distance. The model should also be applicable to fatigue crack analysis in other materials when the required data are obtained.

CONCLUSION

In this research, a model has been developed and described which allows the prediction of true fatigue crack size based on acoustic transmission analysis in aluminum alloys. Additionally, it has been shown that the acoustic wave transmission through a fatigue crack interface as a function of applied stress is very dependent on the interfacial surface roughness when the roughness is below approximately 4.8 μmeters rms, and independent of roughness in the 4.8 μmeter to 10 μmeter rms range. The 10 μmeter rms roughness was the maximum roughness tested and corresponds to measured values from samples fatigued with a constant stress intensity range.

This model should be applicable to fatigue crack analysis in other materials such as steel and titanium when the required data are obtained. The model predicts the crack length independent of relaxation of the crack as long as the general stress dependence across the crack interface remains fixed and the crack surfaces are not totally in contact.

APPENDIX G-1

Evaluation of the integral

$$A = \int_{x=0}^{x} (1-e^{-\alpha x^2})dx$$

The curve of $1-e^{-\alpha x^2}$ describes a normal distribution and must be solved by approximation.

$$A = \int_{x=0}^{x} (1-e^{-\alpha x^2})dx$$

Putting in the finite value of x for the upper limit of integration, let the upper limit be n

$$A = n - \int_{x=0}^{n} (1-e^{-\alpha x^2})dx$$

Let $y = \sqrt{\alpha}x$ then $y^2 = \alpha x^2$

and $dy = \sqrt{\alpha}\, dx$

$$A = n - \int_{0}^{n\sqrt{\alpha}} e^{-y^2} \frac{dy}{d\alpha} = n - \frac{1}{\sqrt{\alpha}} \int_{0}^{n\,\alpha} e^{-y^2} dy$$

Let $z = \sqrt{2y}$ then $z = 2y^2$

and $dz = \sqrt{2}\, dy$

$$A = n - \frac{1}{\sqrt{\alpha}} \int_{0}^{n\sqrt{\alpha}\sqrt{2}} e^{-z^2/2} \frac{dz}{\sqrt{2}}$$

$$A = n - \frac{1}{\sqrt{2\alpha}} \int_0^{n\sqrt{\alpha}\sqrt{2}} e^{-z^2/2}\, dz$$

$$A = n - \frac{1}{\sqrt{2\alpha}} \quad \frac{\sqrt{2\pi}}{1} \left[\frac{1}{\sqrt{2\pi}} \int_0^{n\sqrt{2\alpha}} e^{-z^2/2}\, dz \right]$$

$$A = n - \frac{\sqrt{\pi}}{\sqrt{\alpha}} N\,(n\sqrt{2\alpha})$$

if $\sqrt{2\alpha} > \frac{n}{5}$ then $\alpha > \frac{n^2}{50}$

(1) if $\alpha > \frac{n^2}{50}$ then $A \simeq n - \frac{1}{2}\frac{\sqrt{\pi}}{\sqrt{\alpha}}$

(2) if $\alpha < \frac{n}{50}$ then $A = n - \frac{\sqrt{\pi}}{\sqrt{\alpha}} N(n\sqrt{2\alpha})$

and N must be found in a table for normal distributions.

In the development of the model, α is always greater than $n^2/50$ so the approximation (1) is used.

Communications

Oxygen Transport During Fatigue Crack Growth

J. W. SWANSON AND H. L. MARCUS

It is generally observed that fatigue crack growth rate in an active gaseous environment is higher than growth rate in a baseline vacuum environment.[1,2] It is not clear at this point whether this is a result of interaction at the crack tip in the form of a cyclic stress corrosion or if the gaseous species are transported into the material and internal interaction with the deformation behavior occurs. In the present work, comparison of fatigue crack propagation rates in vacuum and oxygen environments was made for Monel 404,*

*Registered trademark, The International Nickel Company, Inc.

commercially pure titanium, and aluminum 2219-T87 and 7075-T651 alloys (see Table I for compositions). Following the fatigue experiments, samples of the fatigue surfaces were analyzed with Auger Electron Spectroscopy (AES) and Secondary Ion Mass Spectroscopy (SIMS) to determine if oxygen had been transported into the material during crack propagation. The AES measurements were used due to the better spatial resolution and consistent surface chemical sensitivity. The SIMS allowed isotope discrimination during the sputter profiling of oxygen into the bulk.

Compact tension specimens were fatigue cycled through metal bellows in an ion-pumped vacuum chamber. At a pressure of 1.3 μPa (10^{-8} Torr), the crack was grown 0.8 cm with load shedding accomplished each 0.16 cm of growth to maintain the ΔK relatively constant at the value given in Table I. Growth rate was thus established for a vacuum environment. Under constant ΔK conditions, crack growth rate should be constant except for environmental effects, if present. The isotope oxygen-18 of 99.9 pct purity was introduced into the chamber, backfilling to a pressure of 10 kPa (1 kPa for aluminum 2219 due to a limited supply of the isotope). The crack was extended another 0.8 cm at the fixed ΔK and growth rate in the oxygen-18 determined. The specimens were cut and transferred to the AES/SIMS system. Compositional depth profiles of oxygen into the fatigue crack surfaces were then obtained by use of inert ion sputter-etching, combined with AES and SIMS. A more detailed description of the apparatus and procedure can be found in Ref. 3.

The surface formed in vacuum had been exposed to oxygen-18 longer than the surface fatigued in the oxygen-18, since it was formed prior to the introduction of the oxygen-18. It is expected that the profile from the fracture surface formed in vacuum represents simply oxidation and diffusion, while the fracture surface profile from the sample fatigued in oxygen-18 represents oxidation, diffusion, and any additional oxygen transport mechanism occurring during the fatigue crack propagation. Oxidation and diffusion that occurred during transfer from the fatigue chamber to the analysis chamber is in predominantly oxygen-16.

Results of the fatigue crack growth experiments showed an increased crack growth rate in the oxygen environment by a factor of 5 and 2 for Monel and titanium, respectively, with little or no increase apparent for the aluminum alloys. The penetration depth of the oxygen in each case as measured by AES and SIMS is shown in Figs. 1 through 8. It was greater in

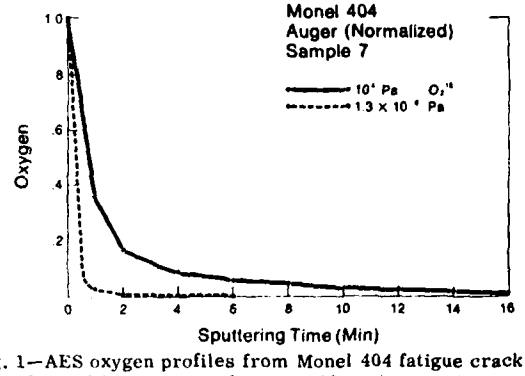

Fig. 1—AES oxygen profiles from Monel 404 fatigue crack surfaces formed in vacuum and oxygen-18 environments.

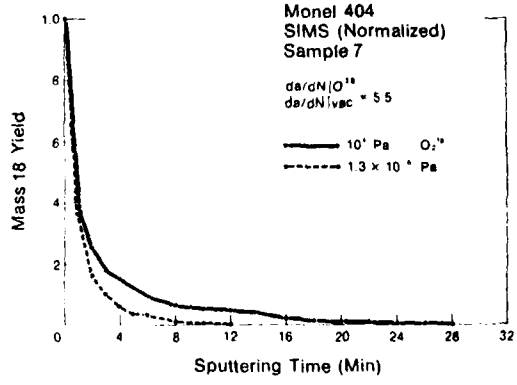

Fig. 2—SIMS oxygen-18 profiles from Monel 404 fatigue crack surfaces formed in vacuum and oxygen-18 environments.

Table I. Nominal Material Compositions and Constant Stress Intensity Range Used in Fatigue Crack Growth Studies

Material	Composition (Pct)	ΔK (MPa $\sqrt{m}$)
Monel 404	52-57 Ni, 0.5 max. Fe, 0.1 max. Mn, 0.15 max. C, 0.024 max. S, 0.1 max. Si, 0.05 max. Al, bal. Cu	33
Titanium	Commercially pure, ASTM B-265 (Gr. 2), 99.2 Ti	22
Aluminum 7075-T651	5.6 Zn, 2.5 Mg, 0.6 Cu, 0.3 Cr, bal. Al	11
Aluminum 2219-T87	6.3 Cu, 0.3 Mn, 0.06 Ti, 0.1 V, 0.2 Zr, bal. Al	11

• SWANSON (formerly Graduate Student in Mechanical Engineering, Materials Science and Engineering, The University of Texas at Austin) is with United States Air Force Academy, Colorado
MARCUS is Professor, Mechanical Engineering, Materials Science and Engineering, The University of Texas at Austin.

ISSN 0360-2133/78/0210-0291$00.75/0

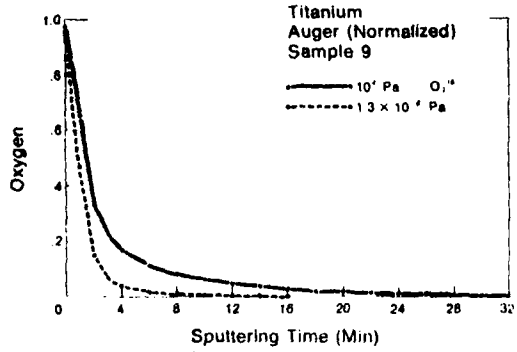

Fig. 3—AES oxygen profiles from titanium fatigue crack surfaces formed in vacuum and oxygen-18 environments.

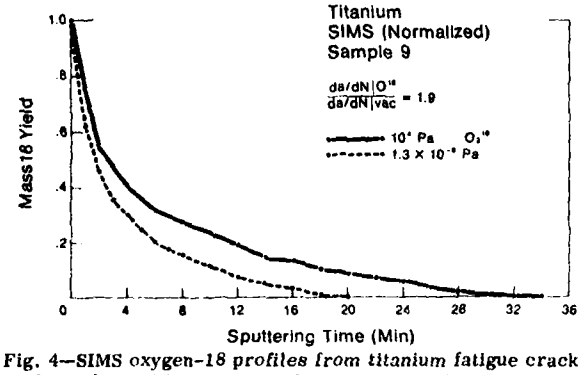

Fig. 4—SIMS oxygen-18 profiles from titanium fatigue crack surfaces formed in vacuum and oxygen-18 environments.

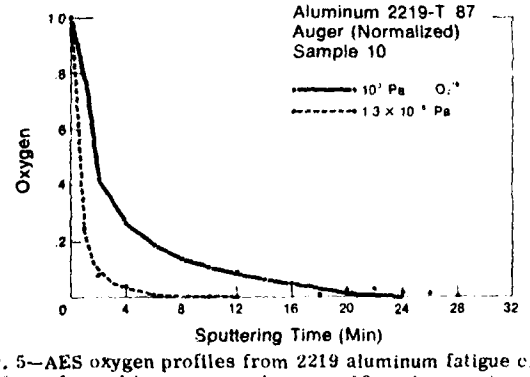

Fig. 5—AES oxygen profiles from 2219 aluminum fatigue crack surfaces formed in vacuum and oxygen-18 environments.

all cases when the crack was grown in oxygen-18. There is consistency between AES and SIMS in indicating enhanced penetration. Limited sputter rate calibration prevents quantification of transport depths, however using an estimated 50 to 100Å for the natural oxide thickness gives an estimate of the enhanced transport of 100 to 600Å.

Samples of metallographically polished Monel and titanium were allowed to oxidize and were sputter profiled using the same ion beam parameters as for the fatigue samples. The profiles thus obtained demonstrated point by point agreement with the samples fatigued in vacuum. This would suggest that changes in surface roughness associated with fatigue crack growth did not contribute significant error to the measurement and could not explain the differences observed in the vacuum and oxygen-18 runs.

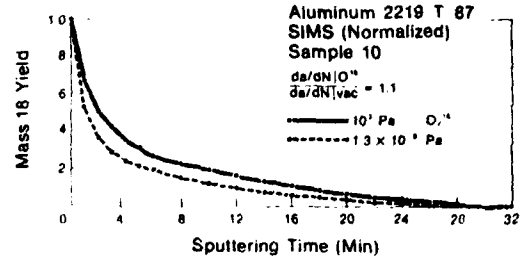

Fig. 6—SIMS oxygen-18 profiles from 2219 aluminum fatigue crack surfaces formed in vacuum and oxygen-18 environments.

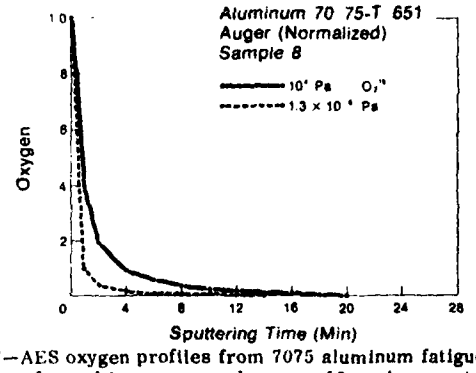

Fig. 7—AES oxygen profiles from 7075 aluminum fatigue crack surfaces formed in vacuum and oxygen-18 environments.

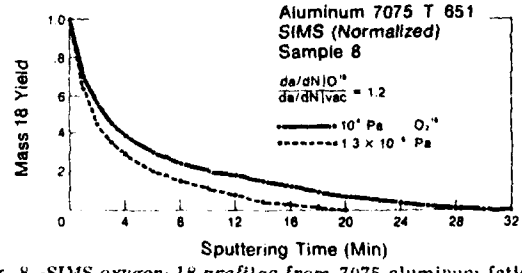

Fig. 8—SIMS oxygen-18 profiles from 7075 aluminum fatigue crack surfaces formed in vacuum and oxygen-18 environments.

From scanning electron micrographs, no change in fracture surface appearance was noted for the aluminum alloys or titanium. The Monel exhibited a large percentage of fracture of a crystallographic nature when fatigued in oxygen, in agreement with previously reported results.[4]

A model for sweep-in of interstitial atoms that originate in the gas phase by mobile dislocations during fatigue crack propagation has been proposed[5,6] and shows the plausibility of such transport for the small hydrogen atom. Using the bulk diffusivity of oxygen, this model is insufficient to explain the present results. If an enhanced oxygen diffusivity near the relaxed high dislocation density surface is postulated, then the dislocation mechanism is plausible.

The interpretation of the fatigue crack growth results by the authors is that gaseous environmental species, oxygen in this case, are transported into the metal during passage of a fatigue crack, possibly by mobile dislocations. The interstitial solute atoms in increased concentrations then interact with the base metal, significantly modifying the local plastic behavior and fracture strain in the vicinity of the crack tip. This interaction for oxygen is apparently the

strongest for Monel 404 and minimal for the alloyed aluminum. The oxygen influence on fracture strain could be the cause for the increase in growth rate. A second possibility would be associated with the crack closure concept[7,8] which is concerned with the fact that during part of the loading cycle the crack closes due to a residual displacement pattern in the wake of the crack. In the case reported here the observed change in oxygen penetration and postulated change in plastic behavior due to the transport of the oxygen could be expected to result in a smaller residual displacement in the wake of the crack, increasing the effective ΔK used in the crack closure model, consequently increasing the growth rate. A great deal of additional research will be required to establish the validity of these hypotheses.

This research is sponsored by the Air Force Office of Scientific Research, Air Force Systems Command, USAF, under Grant No. AFOSR 76-2955. The authors want to thank Dr. P. Lindfours of Physical Electronics for the AES and SIMS analyses.

1. J. D. Frandsen, N. E. Paton, and H. L. Marcus: *Met. Trans.*, 1974, vol. 5, pp. 1655-61.
2. H. L. Marcus, J. C. Williams, and N. E. Paton: *Corrosion Fatigue, NACE-2*, O. F. Deveraux, A. J. McEvily, and R. W. Staehle, eds., 1972, pp. 346-58.
3. J. W. Swanson: "Dislocation Transport of Oxygen During Fatigue Crack Growth," master's thesis, *The University of Texas at* Austin, May 1977.
4. W. L. Morris, J. D. Frandsen, and H. L. Marcus: *Fractography*, ASTM STP, 1976, vol. 600, pp. 49-61.
5. J. K. Tien, A. W. Thompson, I. M. Bernstein, and R. J. Richards: *Met. Trans. A*, 1976, vol. 7, pp. 821-29.
6. J. K. Tien, R. J. Richards, O. Buck, and H. L. Marcus: *Scripta Met.*, 1975, vol. 9, pp. 1097-1101
7. W. Elber: *Eng. Fract. Mech.*, 1970, vol. 2, p. 37.
8. W. Elber: *Damage Tolerance in Aircraft Structures*, ASTM STP, 1971, vol. 486, pp. 230-42.

Appendix I

APPLICATION OF SIMS AND AES TO ENVIRONMENTAL STUDIES OF FATIGUE CRACK GROWTH IN ALUMINUM ALLOYS

Anna K. Zurek and H.L. Marcus
Department of Mechanical Engineering/
Materials Science and Engineering Program
The University of Texas at Austin
Austin, Texas 78712

1. Introduction

The purpose of this investigation was to study the effect of hydrogen, deuterium, water vapor and oxygen on the fatigue crack growth of high strength aluminum alloys. Fatigue crack growth tests in a controlled environment were followed by Secondary Ion Mass Spectroscopy (SIMS) and Auger Electron Spectroscopy (AES).

Influence of humid air on fatigue crack growth in high-strength aluminum alloys is an important practical problem well documented in literature [1-5]. The studies show an increase of crack growth rate of aluminum alloys in water vapor. In many cases it is attributed to hydrogen embrittlement. On the other hand gaseous hydrogen has no effect on fatigue crack growth [4].

Several models of hydrogen embrittlement for various materials have been considered [6-10]. The sweep-in mechanism during fatigue crack growth proposes combination of diffusion and dislocation sweeping of hydrogen into the plastic zone. This results in a hydrogen penetration deeper than $\sqrt{Dt}$, the characteristic depth for diffusion, and a consequent increase in hydrogen concentration that in some manner weakens the material [9,10]. The hydrogen effect is even more pronounced in the presence of various trapping sites such as particle interfaces, which are made more effective by the deformation associated with the propagating crack [9,10,11].

2. Experimental Procedure

The age hardenable aluminum alloys used in this study are 7075-T651 (chemical composition weight percent: 5.6% Zn; 2.5% Mg; 1.6% Cu; 0.3% Cr; and σ_y=505 MPa; K_{IC}=25 MPa$\sqrt{m}$) and 2219-T851 (chem comp.: 6.3% Cu; 0.3% Mn; 0.18% Zn; 0.1% V; 0.06% Ti; and σ_y=350 MPa; K_{IC}=35 MPa$\sqrt{m}$). The compact tension fracture mechanics type specimens were used in the fatigue crack growth experiments [12]. The fatigue crack was first grown in a 1 μPa vacuum at a constant ΔK (ranging from 10 to 21 MPa$\sqrt{m}$) and frequency (6 or 10 Hz). The chamber was then filled with one of the gases hydrogen, water vapor, oxygen-18, deuteriurated water vapor or deuterium gas. Fatigue crack growth was then continued in the environment, up to a certain crack length and then the specimen was fast fractured. Crack propagation rate was monitored optically. Specimens cut from the fracture surfaces were then transferred to AES/SIMS vacuum system. Hydrogen, deuterium and oxygen 18 concentration profiles normal to the fracture surface were investigated by inert ion sputtering combined with SIMS. Negative SIMS was utilized in case of deuterium due to the higher yield of D^- over D^+ ions. For oxygen AES was used in parallel. In addition deuterium ion

implanted standards were prepared using a high energy ion implantation. These were used for calibration purposes of the SIMS system and as a source of measuring induced trapping effects.

3. Results and Discussion

Experimental difficulties were encountered in measuring the atomic hydrogen profile with SIMS in the presence of the $3x10^{-5}$ torr argon sputtering gas. Therefore, oxygen 18 and deuterium as isotope markers in SIMS profiling were used.

Fatigue crack propagation rate for dry oxygen 18 did not significantly increase in comparison to vacuum (1.1 times). The ion sputtering profiles determined by AES and SIMS for 2219 and 7075 aluminum alloys have been published elsewhere [12,13]. A significant enhancement of the thickness of the oxygen for the region fatigued in oxygen 18 by a factor of about 2 to that fatigued in vacuum and subsequently exposed to oxygen 18 occurred in both cases. Dry hydrogen or deuterium also show no change in fatigue crack growth rate when compared to vacuum.

Water vapor (H_2O or D_2O) strongly influences the fatigue crack growth rate. The ratio of crack growth rate in water vapor to that in vacuum varied from 1.8 to 3.6 depending on the ΔK value. The effect was more pronounced for intermediate ΔK values.

The SIMS profile of deuterium in the fracture surface for the specimen tested in vacuum represents deuterium for which diffusion occurred when this surface was exposed to D_2O atmosphere subsequent to the fatigue crack growth (Fig.1, curve 1). The surface profile for the segment cracked in the D_2O vapor represents diffusion and any additional deuterium transport mechanism occurring during the fatigue cycling process (Fig.1, curve 2). Deeper penetration of deuterium for the portion of specimen where fatigue crack growth was in D_2O vapor to that in vacuum was observed (Fig.1). This is in qualitative agreement with dislocation sweeping mechanism [9,10].

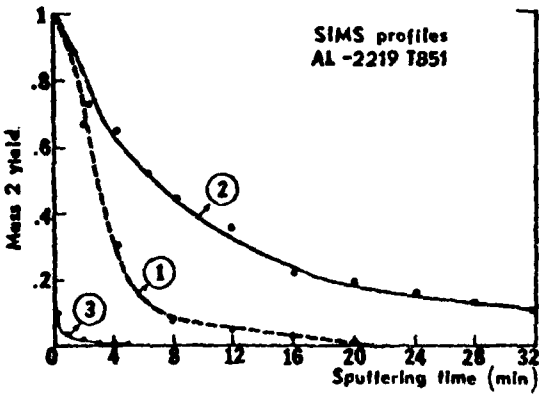

Fig.1 SIMS profiles of D^- in Al-2219 T851 alloy on fractured surfaces and dummy specimen.

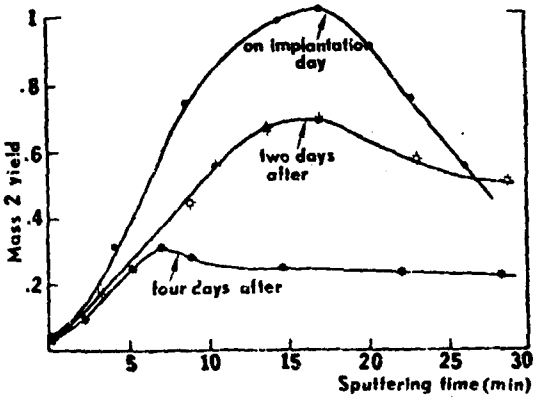

Fig.2 D^- SIMS profiles of deuterium ion implanted Mg-base Mg-Zn alloy.

The deuterium background level in the AES/SIMS system was obtained using the dummy specimen. This specimen was exposed to D_2O environment for the same

period of time as the others but was not fatigued and only a prior existing oxidized surface was exposed. The deuterium SIMS profile from the dummy specimen is initially only about 10% of the signal obtained from the D_2O and vacuum fractured specimens and disappears within 3 to 4 minutes of sputtering time (Fig.1, curve 3). This shows that deuterium contamination from the AES/SIMS vacuum is very low.

Preliminary attempts at calibrating the SIMS system were done on the Mg-base Mg-Zn alloy ion implanted specimens. To simulate the fatigue fracture surface conditions, the specimens were ion bombarded with neon at energies 130 keV and 150 keV. By such multi-implantation, radiation damage was deep and uniform. Then a known dose of deuterium was implanted into the specimen within the damaged region. The profiles of deuterium determined by SIMS are shown in Fig.2. Fig.2 provides two other profiles taken two and four days later. These experiments will be repeated in the near future using aluminum alloys of our interest. Hydrogen implanted into the single crystal of aluminum has been reported to diffuse out within half an hour [15]. Therefore, presence of trapping sites is required for retarding the diffusion of hydrogen and/or deuterium atoms [11,14]. During the deformation associated with the plastic zone of propagating crack in fatigue fractured specimens large amounts of various types of trapping sites are created. Using radiation damage we hope to simulate the destruction of the material of the character created in fatigue fracture. This could then be used to evaluate the hydrogen present and its transport mechanism.

4. Conclusions

(1) SIMS can be applied to study the influence of water vapor on the fatigue crack growth of aluminum alloys. (2) Dry hydrogen (or deuterium) does not affect fatigue crack growth in 2219 and 7075 aluminum alloys. (3) Oxygen penetrates deeper in surfaces formed during fatigue than vacuum fatigued and oxygen exposed surfaces. It does not play a significant role in fatigue crack growth. (4) Hydrogen (or deuterium) from water vapor influences the fatigue crack growth rate and increases penetration of hydrogen and/or deuterium into the material. (5) Ion implanted specimens can be used for the SIMS calibration and for the trapping analysis.

Acknowledgement: This research was sponsored by the Air Force Office of Scientific Research, NE Contract AFOSR 76-2995. The authors want to thank Dr. R. Walser for discussions, Mr. Joe Cecil for preparing the ion implanted specimens and D. Mahulikar for assistance in experimental procedure.

References

1. M. Nageswararao and V. Gerold, 1976, Metallurgical Transactions 7a, 1847.
2. W.L. Morris, 1977, Met. Trans. 8A, 589.
3. J. Steven Enochs and Owen F. Devereux, 1975, Met. Trans. 6A, 391.
4. M.O. Speidel, 1973, Proc. of an Inter. Conf., Champion, Pa., AIME.
5. J. Albrecht, et al., 1977, Scripta Metallurgica V.II, 893.
6. R.A. Oriani, 1972, Technological Aspect 8, 848
7. J. Schijve, 1979, Eng. Fracture Mechanics, V.11, 167.
8. C.D. Beachem, 1972, Met. Trans, 3.
9. J.K. Tien, 1975, Proc. of an Inter. Conf., Moram, Wyoming, AIME.
10. J.K. Tien, et al., 1975, Scripta Metallurgica, 9, 1097.
11. C.A. Wert, 1978 Topics in Applied Physics 29, 305
12. J.W. Swanson and H.L. Marcus, 1977, Met. Trans, 9A, 291.
13. H.L. Marcus, 1977, Environmental Degradation of Eng. Materials Conf., Va.
14. W.M. Robertson, 1979, Met. Trans., 10A, 489.
15. J.P. Bugeat, et al., 1976, Physics Letters, 58A, 127.

Appendix J

SIMS STUDY OF DEUTERIUM TRAPPING IN ION IMPLANTED ALUMINUM ALLOYS

A.K. Zurek*, H.L. Marcus*,
J.N. Cecil** and R. Powers**
*Department of Mechanical Engineering and
Materials Science and Engineering
The University of Texas
Austin, Texas 78712
**Accelerators Incorporated
Austin, Texas 78712

Introduction

The aim of this paper is to report on a deuterium in aluminum trapping inversion experiment. Deuterium ions, deposited at a sharply defined depth by cyclotron irradiation undergo diffusion with reversible trapping. This leads to a gradual redistribution of the deuterium atoms within the metal and their slow evaporation from its surface - an inverse of the usual adsorption and transport mechanism. In this paper, we report and discuss deuterium and oxygen atomic distribution profiles followed by means of SIMS and Auger electron spectroscopy.

The influence of hydrogen on fatigue crack growth in structural aluminum alloys is discussed widely in the literature[1-6]. It has been shown that humid air and water vapor increases crack propagation rate in aluminum alloys but dry hydrogen has no effect[7,8]. At room temperatures, diffusivity of hydrogen in metals is extremely high and exceeds that of heavy interstitials like oxygen and nitrogen by 15 to 20 orders of magnitude[9]. Penetration of hydrogen during

fatigue crack growth could be deeper than the predicted depth for simple diffusion using the sweep-in concept[10,11]. The time scale of hydrogen presence in the metal during fatigue is certainly much longer than characteristic time for hydrogen diffusion[8]. Therefore, a presence of trapping sites for hydrogen must be expected in various forms such as Cottrell atmospheres, interfaces, vacancies, voids, etc.[9-14]. It has been reported that hydrogen implanted into the single crystal of aluminum diffuses out within half an hour[15], less time than it would take to run the fatigue experiment, thereby confirming the need for trapping sites to explain the longer presence of the deuterium. In consequence, a concentration of hydrogen higher than the solubility level in the aluminum alloy associated with trapping sites could be related to the observed increase in the crack propagation rate during the fatigue tests[8].

Materials and Experimental Approaches

Specimens of 2219-T87 and 7075-T6 aluminum alloys were prepared in four different ways. The preparation prior to deuterium implantation included as received unrolled, cold rolled 7-10%, radiation damaged and the fracture surfaces of a sample fatigued in 50% RH laboratory air. Surfaces of the as received unrolled, cold rolled and specimens prepared for the radiation damaged received light polish finish using a soft cloth polishing wheel. The radiation damaged samples

were subjected to the neon irradiation with a beam of 130 KeV and a dose 8 x 10^{15} ions/cm^2 at a projected range of 0.23 μm. Such high energy ion radiation produces point defects (interstitials, vacancies) and vacancy clusters[16]. Slightly higher doses of impinging neon atoms into the prepared aluminum alloy thin disks caused overheating, melting and destruction of the specimen. The specimens were cooled to room temperature before the deuterium implanting process to be described below. Cold rolling produces deformed grains, higher dislocation density, and modified precipitate matrix interfaces. Thus, as a result of increased dislocation density and modified interfaces a cold worked material has a higher possibility of trapping hydrogen than an unrolled one. The fracture surfaces from the fatigued specimens represent a graded deformation process with the largest deformation and corresponding trapping sites expected to be closest to the surface.

Due to the high background level of hydrogen in the AES/SIMS system vacuum chamber, deuterium as an isotope was used to study the trapping mechanism. The deuterium, (D+) implantation (beam of 25 KeV, and a dose 6 x 10^{15} ions/cm^2, at a projected range of 0.24 μm) was done in an AIM 210 Accelerator with 90° magnetic analyzer and energy resolution of 0.04% FWHM. The beam was perpendicular to the implanted surfaces. The deuterium implanted specimens were transferred into the AES-SIMS vacuum chamber. Penetration and time dependent diffusion

profiles of implanted ions and oxygen were obtained using SIMS and Auger Electron Spectroscopy. Due to the experimentally observed higher yield of D^- as compared to D^+, negative SIMS was utilized. The relative yield phenomenon depends on many factors such as ion energy as was observed by others[17]. In addition, platinum masks were used over the specimens to minimize the contribution to the SIMS signal from non-uniformly sputtered edges.

Results and Discussion

The results of the diffusion of the ion implanted deuterium as determined by inert Ar ion sputtering are shown in Figs. 1 and 2. In all cases the concentration after 24 hours is greater in the vicinity of the surface than in the interior. However, there was a small increase in concentration at a certain depth from the surface for neon predamaged samples. Assuming an average inert ion sputtering rate of 200A per min., this depth closely corresponds to the projected range of both implanted ions. This increase in concentration of deuterium at a projected range is due to the locally induced traps formed by the high energy neon irradation. It is highly unlikely that near surface trapping sites were filled starting from the surface during the implantation since no such attenuation process is known to exist for the high energy incident deuterium ions. The binding energies of trapping sites with deuterium for different metals are typically five orders of magnitude smaller than the kinetic

energy of impinging ions[12,13,18,19]. Moreover, a maximum concentration at the expected penetration depth for the neon predamaged specimens is well defined [Fig. 1,2]. Therefore, the initial implanted distribution is that expected by their penetration to the projected range and diffusion of deuterium after implantation must be responsible for the ultimate observed distribution. The relative differences in the final concentrations for the different specimens must be due to the differences in trapping potential. Some quantitative data on trapping energies of different trapping sites is available in literature[13,19]. Second phase particles, solute atoms, low angle grain boundaries and microvoids homogeneously distributed have been considered as strong traps for hydrogen with the highest trapping energies on the order of ~1 eV. Microcracks, large particles and high angle grain boundaries usually heterogeneously distributed are considered as localized traps for hydrogen having an increasing damage effect on the material and trapping energies lower than 0.6 eV. Dislocation and lattice sites are very reversible diffusion sites and are poor traps for the hydrogen with a trapping energy of approximately 0.2 eV. The reported trapping energies[13,19] are not for aluminum alloys. In the case of aluminum the strongest traps should be voids or microcracks where a gas can form which would not tend to dissociate on aluminum resulting in the highest trapping energy. Fatigue fractured surfaces are expected to have the highest density of microvoids, microcracks, grain boundaries and

dislocations with an increasing density of these traps towards the surface. The accumulation of these traps at the surface is expected because of the large strain field formed in the vicinity of the propagating crack due to the crack opening displacement and reverse yielding. In case of cold rolled specimens, near surface accumulation of microcracks, damaged boundaries, precipitate particles and high dislocation density are known to be sinks for hydrogen. The observed lower concentration of deuterium for cold rolled specimens in comparison to fatigue fracture is not surprising due to the presence of lower trapping energy sites. The as received unrolled specimens with fewer and uniformly distributed trapping sites such as second phase particles, small dislocation density and very reversible diffusion lattice sites fall in the third category of the surfaces capable to trap implanted deuterium. The unrolled specimens and the neon radiation predamaged specimens seem to behave identically in terms of the observed near surface concentration profile for deuterium. The light mechanical polishing of the unrolled specimens with and without neon predamage, would be expected to introduce limited amounts of near surface trapping sites.

To explain the results shown in Figs. 1 and 2, samples can be separated into two categories. The first category includes the unrolled specimens with and without neon predamage. In this case the source of the observed profile is

associated with the oxide surface layer acting as a diffusion barrier. The second case is for the fracture surfaces and the cold rolled specimens. In these cases there is a significant introduction of strong traps near the surface but extending interior to the oxide layer. The two cases are discussed separately below.

In the first approximation we can consider the oxide layer formed at the surface of the unrolled and neon predamaged specimens as a barrier for the outdiffusing deuterium. The initial distribution of the deuterium just after the implantation can be represented by:

$$\rho(x,t=0) = \lim_{t\to 0} \frac{1}{\sqrt{\pi Dt}} \exp\left(\frac{-(x-x_o)^2}{4Dt}\right) = \delta(x-x_o) \qquad (1)$$

The increase in the local trapping at the projected range in the neon predamaged specimens would lower the total flux of the diffusing deuterium towards the surface. In further steps we will ignore this local trapping in order to simplify general form of the solution.

We seek solution to the Fick's equation

$$\delta(x,t) = -D \frac{\partial^2 \rho}{\partial x^2} \qquad (2)$$

with the initial condition (1) and a reflecting barrier at $x = 0$:

$$\left.\frac{\partial \rho(x,t)}{\partial x}\right|_{x=0} = 0 \qquad (3)$$

It is customary to dispose of the cumbersome boundary problem by introducing "mirror image" of the initial distribution. This yields as a solution the sum of two Gaussians:

$$\rho(x,t) = \frac{1}{\sqrt{\pi Dt}} \{\exp(-\frac{(x-x_o)^2}{4Dt}) + \exp(-\frac{(x+x_o)^2}{4Dt})\} \qquad (4)$$

which satisfies boundary condition (3). In the region significant for us $x>0$, $\rho(x,t)$ evolves with time in a manner shown in Fig. 3. The solution for time t_4 is what we observed for near surface behavior of the unrolled and neon predamaged specimens first day after the implantation. The second day after the deuterium implantation no traces of deuterium were detected in unrolled and neon predamaged surfaces. Therefore we presume that near surface traps in these specimens must be almost uniformly distributed, reversible and very weak allowing fast diffusion of implanted deuterium within the specimen. Furthermore, the thin oxide formed at these surfaces is a strong barrier for the outdiffusing deuterium.

In the second case as the deuterium diffuses towards the surface in the cold rolled and fatigued specimens it gets trapped in the high binding energy traps extending their presence much deeper than just the oxide layer. Therefore the preceding

AD-A082 526 TEXAS UNIV AT AUSTIN F/G 11/6
THE INFLUENCE OF HOLD TIMES ON FATIGUE CRACK GROWTH OF ALUMINUM--ETC(U)
FEB 80 H L MARCUS AFOSR-76-2955
UNCLASSIFIED AFOSR-TR-80-0233 NL

END
DATE FILMED
5-80
DTIC

analysis will no longer predict the diffusion profile but a more complex analysis including the nonuniform distribution of traps must be used.

Traces of implanted deuterium were observed in the cold rolled specimens up to the fifth day after implantation took place. Afterwards, up to the 14th day, only fatigue fractured specimens showed remaining concentrations of deuterium. Previously discussed strong traps present in the surfaces of these two specimens are responsible for such a long lasting presence of the implanted deuterium. Deuterium profiles obtained with SIMS have been shown[8] for the segment of specimen fatigue fractured in a deuteriunated water vapor environment. In this case, dissociated deuterium entered into the bulk of the material through the free metal surface exposed during the fatigue process. Deuterium gets trapped in a number of high energy trapping sites created during the fatigue fracture process. The immediate formation of the oxide layer slows down the back transport of the deuterium to the surface where evaporation takes place. Deuterium concentration profiles obtained from these specimens and fatigue fractured implanted specimens showed detailed similarities. Both show a high concentration of deuterium at the surfaces and a significant concentration level of deuterium extending into the material much deeper than the observed oxide layers.

This observation suggests that the final distribution of deuterium in the specimens fatigue fractured in the D_2O

environment and ion implanted fatigue fractured surfaces strongly depends on trapping sites formed in the fatigue process.

The oxide-metal interface seems to play another important role for deuterium trapping which is especially pronounced for the fatigue fractured specimens of the 7075-T6 alloy. Fig. 4 shows the correlation between oxygen sputtering profile obtained using AES parallel to deuterium profile utilized from SIMS. At the oxide metal interface a significant buildup of deuterium ions was observed suggesting again an oxide to be a barrier and a oxide-metal interface serving as a strong trap.

Conclusions

1. Large amounts of strong deuterium trapping sites close to the surface are created during the deformation associated with fatigue crack propagation process in aluminum alloys.
2. Deuterium profiles of D_2O vapor fatigue fractured specimens were closely duplicated by trapping inversion experiment. Strong dependence of deuterium distribution with the presence of trapping sites created during the fatigue fracture process was observed.
3. Surface oxides and the oxide-metal interface trap deuterium slowing down the transport to the surface where evaporation takes place.

4. High energy neon radiation induced damage produces weak trapping sites for deuterium.

Acknowledgements

This research was sponsored by AFOSR grant number 76-2955. Discussions with Dr. W.H. Zurek, Dr. R.M. Walser and Dr. J.P. Stark are greatly appreciated.

References

1. J. Albercht, et al: Scripta Met, 1977, vol. 11, p. 893.
2. J. Steven Enochs and Owen F. Devereux: Met. Trans. A, 1975, vol. 6A, p. 391.
3. W.L. Morris: Met. Trans. A., 1977, vol. 8A, p. 589.
4. M. Nageswararao and V. Gerold: Met. Trans. A., 1976, vol. 7A, p. 1847.
5. J.D. Frandsen and H.L. Marcus: Proc. of an International Conference - AIME, Moram, Wyoming, pp. 233-249, 1975.
6. H.H. Johnson: Hydrogen in Metals, ASM: Metals Park, Ohio, pp. 35-49, 1974.
7. M.O. Speidel: Proc. of an International Conference - AIME Champion, PA, pp. 249-277, 1973.
8. A.K. Zurek and H.L. Marcus: Proc. of an International Conference, Stanford, CA, pp. 163-166, 1979.
9. J. Volkl and G. Alefeld, Hydrogen in Metals I, pp. 321-348, Springer-Verlag, 1978.
10. J.K. Tien, et al: Proc. of an International Conference-AIME Moram, Wyoming, pp. 309-321, 1975.
11. J.K. Tien et al: Scripta Met, vol. 9, p. 1097, 1975.
12. G.M. Pressouyre and I.M. Bernstein: Met. Trans. A., vol. 9A, p. 1571, 1978.
13. Ch. A. Wert: Hydrogen in Metals II, pp. 305-330, Springer-Verlag, 1978.
14. W.M. Robertson: Met. Trans. A., vol. 10A, p. 489, 1979.
15. Y.P. Bugeat et al: Physics Letters, vol. 58A, p. 127, 1976.
16. M. Wiedrsick and P.R. Okonato: Interfacial Segregation, pp. 405-432, ASM: Metals Park, OH, 1977.
17. Ming L. Yu: Nuclear Instruments and Methods, 1978.
18. Anton J. West and MacIntyre R. Louthan, Jr.: Met. Trans. A., vol. 10A, p. 1723, 1979.
19. G.M. Pressouyre and I.M. Bernstein: Acta Met., vol. 27, p. 89, 1979.

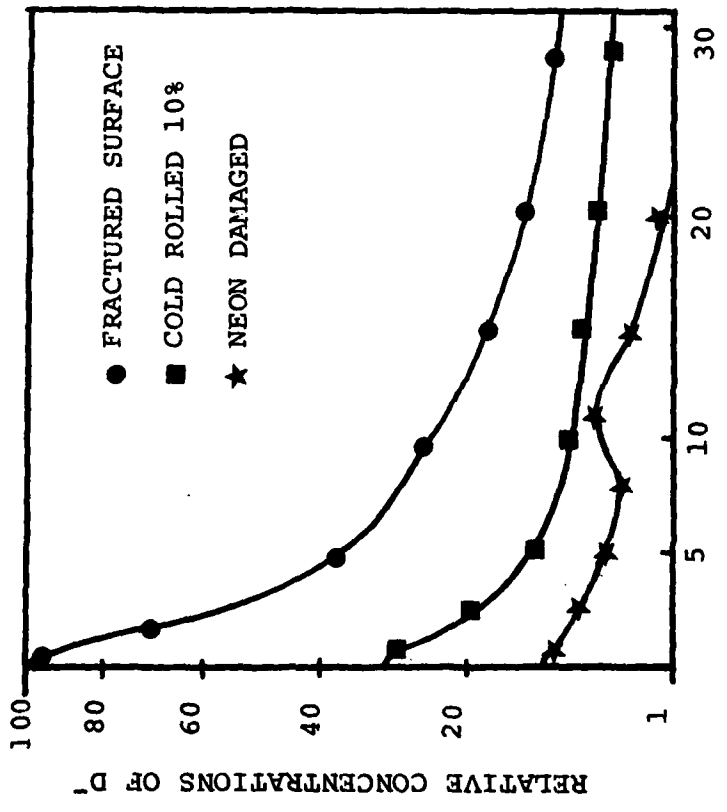

Fig. 1. Deuterium concentration profiles obtained by SIMS for 2219-T87 aluminum alloy, one day after the implantation time.

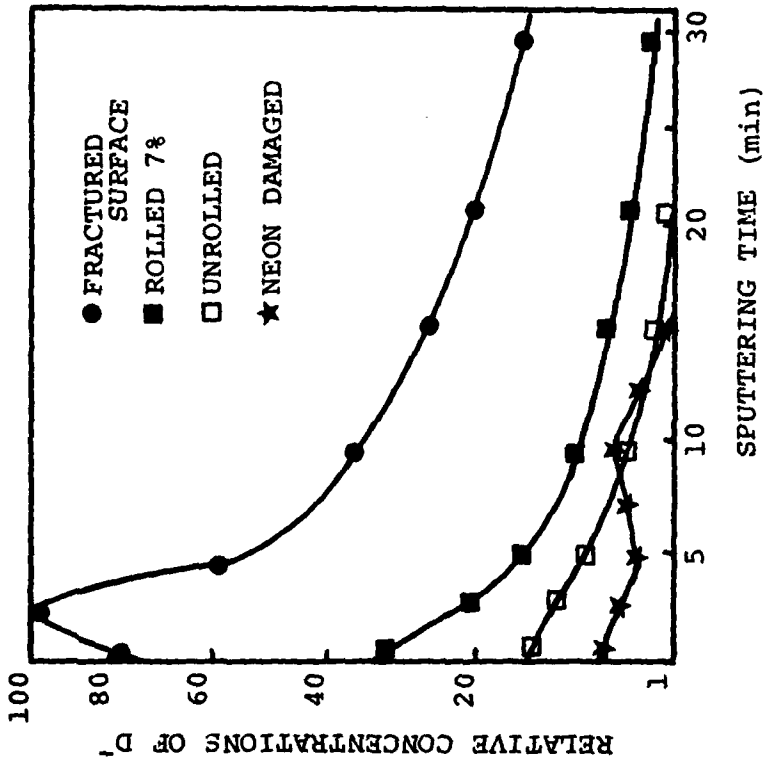

Fig. 2. Deuterium concentration profiles obtained by SIMS for 7075-T6 aluminum alloy, one day after the deuterium implantation.

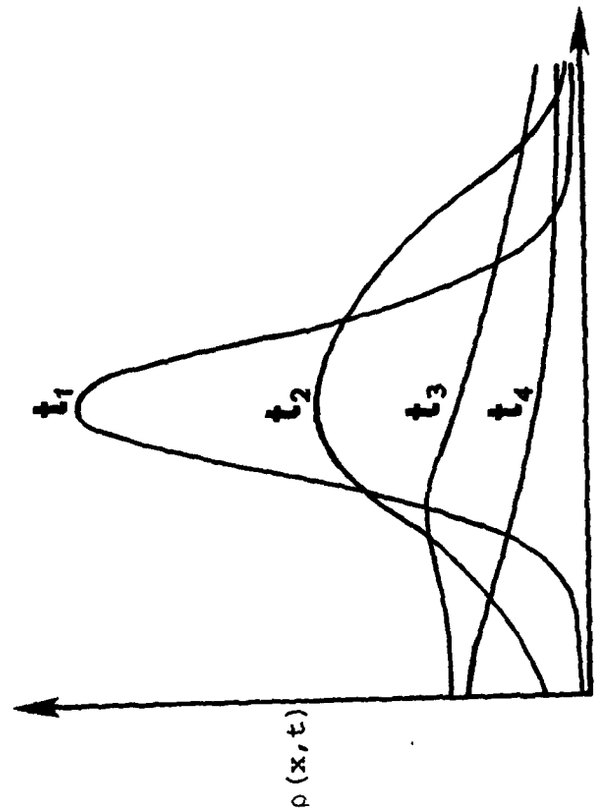

Fig. 3. Concentration profiles evolving in time according to equation 4.

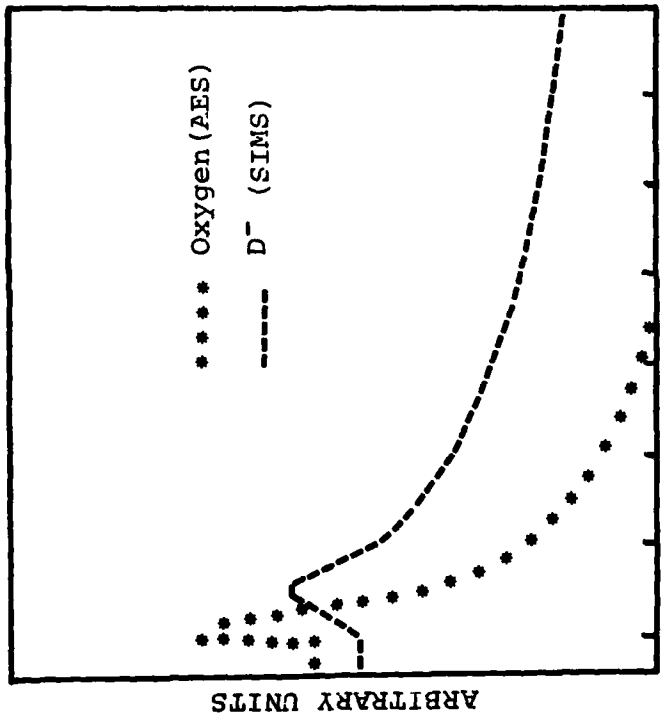

Fig. 4. Oxygen yield obtained by AES and deuterium yield obtained by SIMS from the 7075-T6 aluminum alloy, fatigue fractured surface.

Publication List

1. G. Sewell and H.L. Marcus, "The Influence of Underload Time On Crack Growth Retardation of Aluminum Alloys." Int. J. Fracture 13, 247 (1977). (Appendix A.)

2. W. Slagle, Deepak Mahulikar, H.L. Marcus, "Effect of Hold Times on Crack Retardation in Aluminum Alloys," Submitted for publication to Int. J. Fracture. (Appendix B.)

3. G. Sewell and H.L. Marcus, "A Model For Fatigue Crack Closure Based on Surface Roughness and Residual Strain," Scripta Met. 11, 521 (1977). (Appendix C.)

4. Deepak Mahulikar and H.L. Marcus, "Fatigue Crack Closure and Residual Stress Measurements on Aluminum Alloys," Submitted for publication to Met. Trans. A. (Appendix D.)

5. Deepak Mahulikar, W.P. Slagle and H.L. Marcus, "Edge Effects on Fatigue Crack Closure of Aluminum Alloys," Scripta Met 13, 867 (1979). (Appendix E.)

6. J. Jeffries, H.L. Marcus and O. Buck, "The Influence of Fatigue Crack Surface Roughness on Acoustic Wave Transmission," Proc. 11th Symp. on NDE, ASNT and SRI, San Antonio, TX 275 (April 20-22, 1977). (Appendix F.)

7. J. Jeffries, "Development of a Model to Predict True Fatigue Crack Size Using Acoustic Wave Transmission," from Master's Thesis, University of Texas, Austin, TX, pp. 17 - 32 (1979). (Appendix G.)

8. J. Swanson and H.L. Marcus, "Oxygen Transport during Fatigue Crack Growth," Met. Trans. A., 8A, 291 (Feb. 1978). (Appendix H.)

9. A. Zurek and H.L. Marcus, "Application of SIMS and AES to Environmental Studies of Fatigue Crack Growth in Aluminum Alloys," Proc. IInd International Conf. on SIMS II, Stanford CA 163 (August 27-31, 1979). (Appendix I.)

10. A. Zurek, H.L. Marcus, J. Cecil and R. Powers, "SIMS Study of Deuterium Trapping in Ion Implanted Aluminum Alloys," Submitted for publication to Met. Trans. A. (Appendix J.)

Review Papers

11. H.L. Marcus, "Gaseous Environmental Effects on Fatigue Crack Growth," Proc. Conf. Environmental Degradation of Engineering Materials, Virginia Polytechnic Institute 41 (Oct. 10-12, 1977).

12. H.L. Marcus, "Environmental Effects II: Fatigue Crack Growth in Metals and Alloys," ASM Mat. Sci. Seminar " Fatigue and Microstructure", St. Louis, MO, ASM 365 (Oct. 14-15, 1978).

13. H.L. Marcus, "Subcritical Crack Growth and Its Relation to Predictive Analysis," Proc. ARPA/AFML Review of Progress in Quantitative NDE, La Jolla, CA, 1979.

Theses and Dissertations

14. G. Sewell, "Relaxation and Crack Closure Effects on Fatigue Crack Growth in Al 2219," Master's Thesis, University of Texas, Austin 1978.

15. J. Swanson, "Dislocation Transport of Oxygen During Fatigue Crack Growth," Master's Thesis, University of Texas, Austin 1977.

16. W. Slagle, "Influence of Yield Strength and Environment on Relaxation Effects in Fatigue Crack Propagation," Master's Thesis, University of Texas, Austin 1979.

17. J. Jeffries, "A Model for the Prediction of Fatigue Crack Size Based on Acoustic Interrogation," Master's Thesis, University of Texas, Austin 1979.

18. A. Debogorska (Zurek), "Mechanism of Gaseous Environmental Embrittlement During the Fatigue Crack Growth in Aluminum Alloys," Ph.D. Dissertation, University of Texas, Austin 1980.